EES Batteries

99.99%

99.90%

CE

ROYAL SOCIETY
OF **CHEMISTRY**

REVIEW ARTICLE
Xue-Qiang Zhang, Jia-Qi Huang *et al.*
Advances in high-coulombic-efficiency lithium metal anodes
under practical conditions in liquid electrolytes

Advances in high-coulombic-efficiency lithium metal anodes under practical conditions in liquid electrolytes

Shu-Yu Sun,[a] Xue-Qiang Zhang, ⓘ *[b,c] Xue-Yi Yan,[b,c] Zhao Zheng,[a] Qian-Kui Zhang[a] and Jia-Qi Huang ⓘ *[b,c]

Lithium (Li) metal batteries are regarded as the forefront of high-energy-density battery technology, surpassing the performance of traditional Li-ion batteries. However, their cycle life is notably impeded by the suboptimal coulombic efficiency (CE) of Li metal anodes. CE serves as a pivotal metric for the reversibility of Li plating and stripping processes. The low CE stems from the generation of inactive Li, a phenomenon exacerbated by practical operational conditions. Improving CE is paramount for the practical applications of Li metal batteries. It is crucial to comprehend the genesis of inactive Li and to devise effective strategies aimed at achieving high CE. This review delves into the core principles of CE, its significance across various battery configurations, methodologies for calculation, the pivotal factors influencing CE, and the underlying mechanisms for its enhancement. Subsequently, the review summarizes the advancements in achieving high-CE Li metal anodes under practical conditions, examining both composite Li anodes and electrolyte engineering strategies. Finally, the discussion turns to the challenges and prospective research avenues for enhancing the CE of Li metal anodes under practical conditions in liquid electrolytes, with the ultimate goal of realizing viable Li metal batteries.

Broader context

Lithium (Li) metal batteries, renowned for their high energy density, are being revived as leading contenders for next-generation batteries. However, their widespread commercial adoption is hampered by the short lifespan of Li metal anodes, which is attributed to poor coulombic efficiency (CE). This inefficiency is primarily caused by the accumulation of inactive Li and undesirable side reactions with the electrolyte at the anode, which are particularly exacerbated under practical conditions. Researchers have endeavored to enhance the CE of Li metal anodes through innovative electrolyte engineering and composite anodes. Despite these efforts, there is a noticeable scarcity of literature that provides a comprehensive analysis of CE under practical conditions. The purpose of this review is to offer a systematic and timely discussion of the advances of the CE of Li metal anodes under practical conditions from the perspective of a basic understanding and technical methods, and to provide forward-looking insights to promote the development of high-CE Li metal anodes under practical conditions in the future.

1 Introduction

Lithium (Li) batteries are increasingly pivotal in the quest for a zero-carbon, wireless world, serving as portable energy storage

[a] Tsinghua Center for Green Chemical Engineering Electrification & Beijing Key Laboratory of Complex Solid State Batteries, Department of Chemical Engineering, Tsinghua University, Beijing 100084, P. R. China
[b] Advanced Research Institute of Multidisciplinary Science, Beijing Institute of Technology, Beijing 100081, P. R. China
[c] School of Materials Science and Engineering, Beijing Institute of Technology, Beijing 100081, P. R. China

solutions.[1–4] The surging demands of electric vehicles and portable devices necessitate high-energy-density batteries.[5–8] Despite considerable progress, the energy density of commercial Li-ion batteries based on intercalation chemistry is approaching the ceiling of 350 Wh kg^{-1}.[9–12] Since the 2010s, there has been a resurgence in interest in Li metal batteries, which leverage conversion chemistry and hold the promise of achieving energy densities surpassing 500 Wh kg^{-1}.[13–18] However, the practical applications of Li metal batteries are impeded by their limited cycle life and even safety risks. The poor reversibility of Li metal anodes, resulting from high reactivity and non-uniform plating/stripping behaviors, are key

factors that deteriorate battery performance.[19–22] These challenges are magnified when Li metal anodes are operated under practical conditions, posing notable obstacles to their commercialization.

Coulombic efficiency (CE) is a key indicator of the reversibility of Li plating and stripping on the anode, illuminating the consumption of active Li on the anode side.[23–26] CE is defined as the ratio of the capacity of Li that can be stripped to the capacity of Li that has been deposited on the current collector in each cycle.[27–31] A low CE means there is much inactive Li formed during each cycle. Moreover, the continuous accumulation of inactive Li leads to increased interfacial resistance on the anode side, which is unfavorable for stable Li metal batteries.[32–37] Therefore, a high CE of Li metal batteries, especially under practical conditions, is vital for achieving long-cycle-life Li metal batteries.

Low CE is primarily driven by the formation of inactive Li. Inactive Li results from two key issues: the formation of Li^0 and the repeated formation of the solid electrolyte interphase (SEI) through the accumulation of Li^+.[38–40] During Li plating, the uneven transport of Li ions in the SEI results in dendritic Li deposition on the current collector. These dendrites are particularly susceptible to breaking off at their root during Li stripping, leading to a loss of electrical connection with the current collector and subsequent transformation into unusable inactive Li^0 for future cycles.[41–43] Moreover, the inherently unstable SEI is prone to fracturing under substantial volume fluctuations during the Li plating/stripping process, which exposes highly reactive Li to the electrolyte. This exposure triggers additional side reactions with the electrolyte, leading to the formation of a new SEI and the depletion of active Li capacity.[44–46] In addition to the reconstruction of the SEI occurring during the Li plating and stripping process, the porous SEI makes it susceptible to electrolyte permeation even under open-circuit con-

ditions; this leads to ongoing SEI growth and continuous capacity consumption.[47–49]

In the pursuit of high-CE Li metal anodes under practical conditions, the primary focus has been on reducing the formation of inactive Li^0 and preventing capacity loss due to the repeated formation of the SEI.[50–52] Dominant strategies are centered on the development of composite Li anodes and electrolyte engineering. Composite Li anodes leverage functional hosts to minimize dendritic Li growth, thereby reducing the generation of inactive Li^0.[53,54] In parallel, electrolyte engineering employs functional electrolytes to regulate the properties of the SEI, enhancing its uniformity and stability. Electrolyte engineering ensures a uniform deposition pattern of Li and mitigates capacity loss stemming from the repeated formation of the SEI.[55–57] After years of dedicated refinement, Li metal anodes have achieved an impressive CE of 99.9% under mild conditions. However, it is essential to strive for a CE exceeding 99.99% under practical conditions in order to ensure the stability of Li metal anodes during long cycles.[58–60] Consequently, a huge challenge lies ahead in the ongoing development of high-CE Li metal anodes under practical conditions, highlighting the necessity for relentless innovation.

The aim of this review is to provide a comprehensive account of the progress made in the development of high-CE Li metal anodes under practical conditions in liquid electrolytes. The article first emphasizes the importance of CE in Li metal anodes under practical conditions and provides an overview of the methods used to calculate CE in different battery configurations. The review then summarizes recent progress in the development of high-CE Li metal anodes under practical conditions, with particular emphasis on composite Li anodes and electrolyte engineering. Finally, the review presents a prospective outlook for future research, emphasizing strategies to improve the CE of Li metal anodes under practical conditions.

Shu-Yu Sun received his bachelor's degree from the Department of Chemistry at Tsinghua University in 2021. Presently, he is a Ph.D. candidate in the Department of Chemical Engineering at Tsinghua University under the supervision of Prof. Qiang Zhang. His research interests focus on the ion transport properties and stability of anode/electrolyte interfaces in lithium batteries.

Shu-Yu Sun

Xue-Qiang Zhang received his bachelor's degree from Tianjin University and Ph.D. degree from Tsinghua University. He is currently an assistant professor at the Advanced Research Institute of Multidisciplinary Science (ARIMS) in the Beijing Institute of Technology. His research interests focus on the electrochemical model of an anode/non-aqueous electrolyte interface and the corresponding strategies to stabilize the interface in secondary batteries, especially next-generation high-energy-density batteries.

Xue-Qiang Zhang

2 Coulombic efficiency (CE) in Li batteries

2.1 The challenge of high CE under practical conditions

To bring Li metal batteries to the forefront of commercialization, it is crucial to outperform the energy density of cutting-edge Li-ion batteries (300 Wh kg^{-1}).[61–63] In the optimal scenario, the energy density of a Li metal pouch cell can surpass 500 Wh kg^{-1}.[64,65] Jiao and co-workers identified a strategy to achieve a pouch cell with an energy density exceeding 500 Wh kg^{-1}.[66] For a pouch cell with an energy density above 500 Wh kg^{-1}, a Li metal anode with limited thickness (less than 50 μm, translating to an areal capacity of less than 10.0 mAh cm^{-2}), a cathode with a high areal capacity (more than 5.0 mAh cm^{-2}, ensuring the negative to positive ratio (N/P ratio) is less than 2.0), and lean electrolyte conditions (electrolyte to capacity ratio (E/C ratio) below 1.5 g Ah^{-1}) are necessary. Furthermore, to ensure competitiveness, the charging/discharging current density of Li metal batteries should exceed 1.0 mA cm^{-2}, as illustrated in Fig. 1a.

Nevertheless, in comparison with the relatively mild conditions typically employed in the context of coin cells, it is considerably more challenging to attain a high CE under practical conditions that are oriented towards high energy density in Li metal batteries.[53,67–69] Under practical conditions, the Li reservoir of the anode is significantly constrained by the requirement for a low N/P ratio. In systems with an N/P ratio of less than 1.5, there is a reservoir of merely 50% excess Li, with the capacity of each cycle occupying a minimum of two-thirds of the overall Li reservoir on the anode side. This indicates that in the event of significant irreversible capacity loss on the anode side, the Li reservoir of the anode side will be depleted rapidly, resulting in a rapid capacity decay and significant challenges in achieving a high CE. Moreover, the volume of electrolyte is significantly diminished under practical conditions, comprising less than one-tenth of the corresponding volume in the coin cells under mild conditions (E/C ratio >20 g Ah^{-1}). In this case, the amount of electrolyte is insuffi-
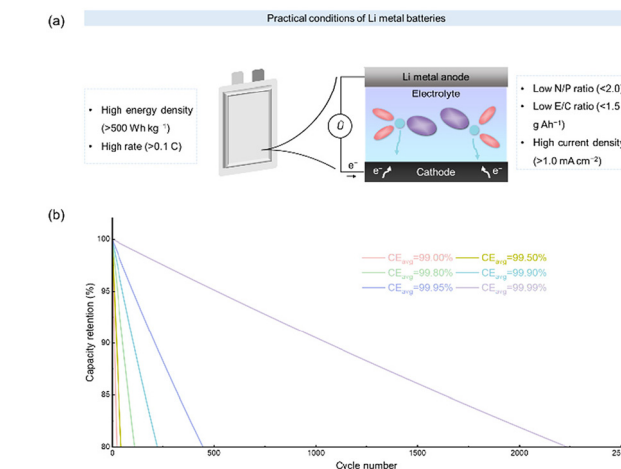

Fig. 1 (a) The practical conditions of high-energy-density Li metal batteries. (b) Effect of coulombic efficiency (CE) on the cycle life of anode-free Li metal batteries.

cient, while the charging capacity of the cycle is larger, resulting in a further increase in electrolyte consumption due to side reactions on the anode side in each cycle. In the case of the total amount of electrolyte, the increase in consumption per cycle will lead to the rapid depletion of electrolyte in the battery, resulting in failure of the battery and difficulties in achieving high CE.

For anode-free Li metal batteries, the absence of a Li reservoir on the anode side results in a further acceleration of the failure rate of Li metal batteries due to the consumption of the Li reservoir and electrolyte. Consequently, the challenge of achieving a high CE under practical conditions is undoubtedly the most formidable.[23,70,71] Conversely, the lack of Li reserves results in the capacity of the battery being directly contingent upon the remaining capacity of the cathode. Consequently, for the anode-free Li metal battery, the CE is a determining factor in the cycle life of the battery. When the CE of the cathode is nearly 100% and the capacity retention is 80%, an anode-free

Xue-Yi Yan received her bachelor's degree from Beijing Institute of Technology in 2024. Presently, she is a master's student at the Beijing Institute of Technology under the supervision of Prof. Xue-Qiang Zhang. Her research interests focus on the stability of the lithium anode/electrolyte interface in lithium metal batteries.

Xue-Yi Yan

Jia-Qi Huang is a professor at the Advanced Research Institute of Multidisciplinary Science of the Beijing Institute of Technology. He received his bachelor's and Ph.D. degrees from the Department of Chemical Engineering at Tsinghua University. His research group focuses on interfacial electrochemistry and material designs in high-energy-density rechargeable batteries, especially for lithium–sulfur batteries and lithium-metal anodes.

Jia-Qi Huang

Li metal battery with a CE of 99.00% endures for 22 cycles. Conversely, a battery with a CE of 99.99% can achieve up to 2231 cycles, as illustrated in Fig. 1b. For full cells incorporating Li metal anodes, CE is not the sole determinant of cycle performance. However, the utilization of Li metal anodes with a high CE substantially mitigates electrolyte consumption and irreversible capacity loss, thereby bolstering the stability of longer cycling.[67,72–74] Consequently, high CE emerges as a pivotal factor for ensuring the extended lifespan and elevated energy density of Li metal batteries under practical conditions.

2.2 The CE in various cell configurations

It has been highlighted that the CE of an anode serves as a pivotal parameter for evaluating the stability of Li plating and stripping processes on the anode. Nonetheless, it is imperative to acknowledge that the CE measured in different cell configurations is not indicative of the CE of the anode side. To elucidate the factors contributing to anode failure, it is essential to conduct an in-depth analysis of how CE mirrors the working status of batteries in various cell configurations.

In the context of a half-cell, as represented by the Li|Cu cells, the degradation of CE is a direct indicator of the lifespan of batteries, given the substantial surplus of Li on the anode.[75,76] The decline in CE mirrors the reversibility of Li plating and stripping processes at the cathode. Generally, CE unfolds in two distinct stages, as illustrated in Fig. 2a and b, which reflect the evolving surface conditions of the cathode. In the nascent state of stage I, the SEI on the cathode is growing and thickening, which leads to a subdued initial CE and then gradually ascends upon stabilization of the SEI. With a stable SEI, the accumulation of highly resistive inactive Li and SEI is

minimal, inducing a low overpotential for Li plating and stripping, thus stabilizing the CE. However, as the system progresses to stage II, the relentless accumulation of inactive Li and SEI intensifies, ultimately blanketing the surfaces of both electrodes. The emergence of these highly resistive layers hampers the efficient stripping of Li from the cathode, triggering a precipitous drop in CE.

When it comes to the full cells, like Li|LiNi$_x$Co$_y$Mn$_z$O$_2$ (NCM, with $x + y + z = 1$), CE is influenced not just by the anode but also significantly by the cathode, which means that the CE of full cells is not the only factor that determines the lifespan of Li metal batteries.[27,73,77] Consequently, capacity retention and the CE of Li metal batteries exhibit a two-stage trend, as illustrated in Fig. 2c and d. In the first stage, the reservoir of surplus Li present in the anode ensures that the cathode is fully discharged in each cycle. This is achieved by excess Li compensating for the irreversible capacity loss occurring on the anode side. During this stage, the CE and capacity of full cells remain relatively stable, with the CE of the battery mirroring the CE of the cathode being dictated by the cathode structure. As the second stage is reached, the Li reservoir of the anode is depleted, resulting in the CE of full cells being controlled by the CE of the anode. Therefore, the cathode is disabled to be fully discharged during each cycle, leading to a continuous decline of capacity and CE of full cells due to ongoing irreversible capacity loss at the anode.

For anode-free Li metal batteries, similar behavior for the CE change is observed. There is no Li reservoir on the anode side in the initial stage. After the first charge/discharge cycle, deposited Li cannot be fully discharged to the cathode owing to irreversible lattice collapse. Thus, residual deposited Li is
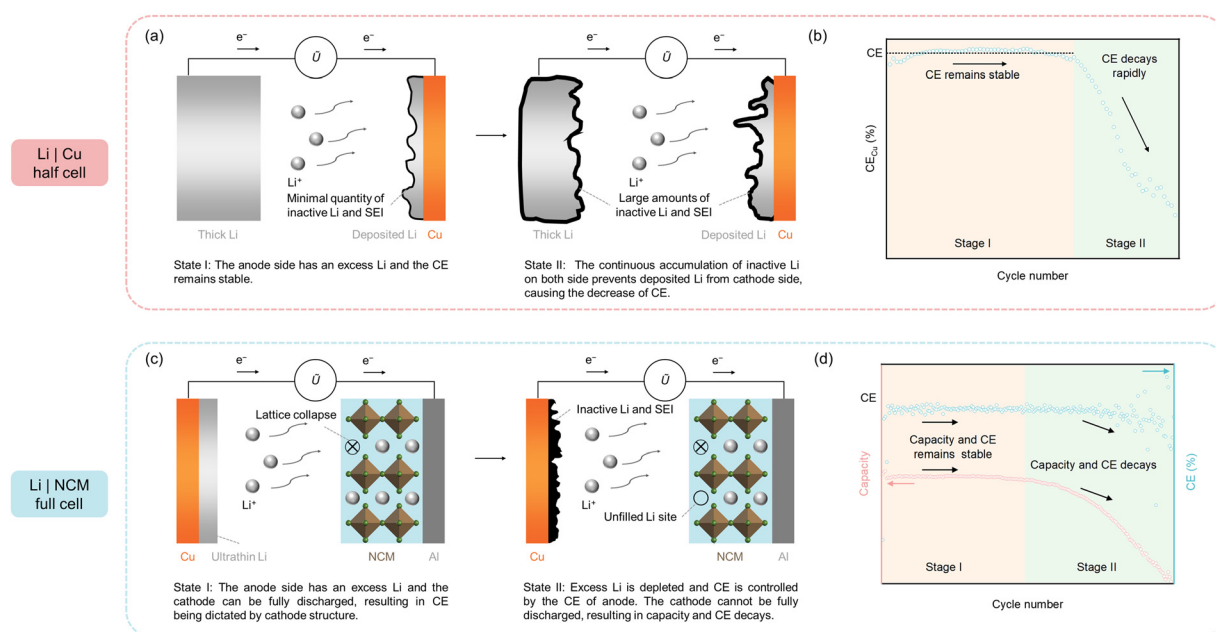

Fig. 2 The evolution of CEs and capacity with cycles in various cell configurations. The diagram of the changes of CE and capacity retention during cycling in (a) Li|Cu half cells and (c) Li|NCM full cells. The curves of the changes of CE and capacity retention during cycling in (b) Li|Cu half cells and (d) Li|NCM full cells.

accumulated on the anode side as the Li reservoir. Consequently, the configuration of anode-free Li metal batteries is transformed to normal Li metal batteries with a reservoir of excess Li. The capacity and CE of anode-free Li metal batteries exhibit trends analogous to those of normal Li metal batteries. However, given that the reservoir of excess Li on the anode side in anode-free Li metal batteries is smaller than that in normal Li metal batteries, the turning point in stage II will occur earlier.

2.3 Calculation methods for the CE

It is essential to accurately quantify the CE of Li metal anodes to ensure a fair comparison. This section is dedicated to a comprehensive analysis of the methodologies employed for CE measurement in a variety of settings. It comprises a comprehensive analysis of the fundamental principles that underpin these methodologies, a synthesis of their evolutionary pathways, and a critical evaluation of inherent advantages and limitations associated with each technique.

2.3.1 Half cells. In the scholarly discourse surrounding Li-ion batteries, CE is conventionally delineated as the quotient of the discharge capacity to the charge capacity at a specified electrode. However, within the context of half-cell configurations, the CE is articulated as the ratio of Li stripped from the Cu substrate to Li plated on the Cu substrate previously, as encapsulated in eqn (1).

$$CE_{Cu} = \frac{Q_{stripping}}{Q_{plating}} \quad (1)$$

Notwithstanding the considerable advances that have been made in the methodology of testing CE, the fundamental tenet of the testing procedure remains inextricably linked to the equation.

Conventional method. In the conventional method for assessing CE, the process begins with the controlled deposition of a specified quantity (Q_p) of Li onto the Cu substrate. Thereafter, a specific positive stripping cut-off voltage (typically +1 V) is applied to ensure that the entirety of removable Li (Q_s) is effectively stripped from the Cu substrate, as depicted in Fig. 3a. Given a defined number of cycles (n), the average CE is then calculated using eqn (2), which quantifies the electrochemical reversibility of the Li plating and stripping processes on the Cu substrate over the specified cycles.

$$CE_{avg} = \frac{1}{n}\sum\frac{Q_s}{Q_p} \quad (2)$$

This method, widely embraced by the scientific community, owes its popularity to inherent simplicity, as exemplified by the representative curve presented in Fig. 3d. It is of utmost importance to emphasize the critical necessity of maintaining a substantial excess of Li on the counter electrode in order to prevent potential inaccuracies in CE measurements.[75] Despite the apparent simplicity of the conventional method, it is of paramount importance to acknowledge that the absence of the SEI on the initial substrate necessitates a period of stabilization for CE during the initial cycles. This initial phase is criti-
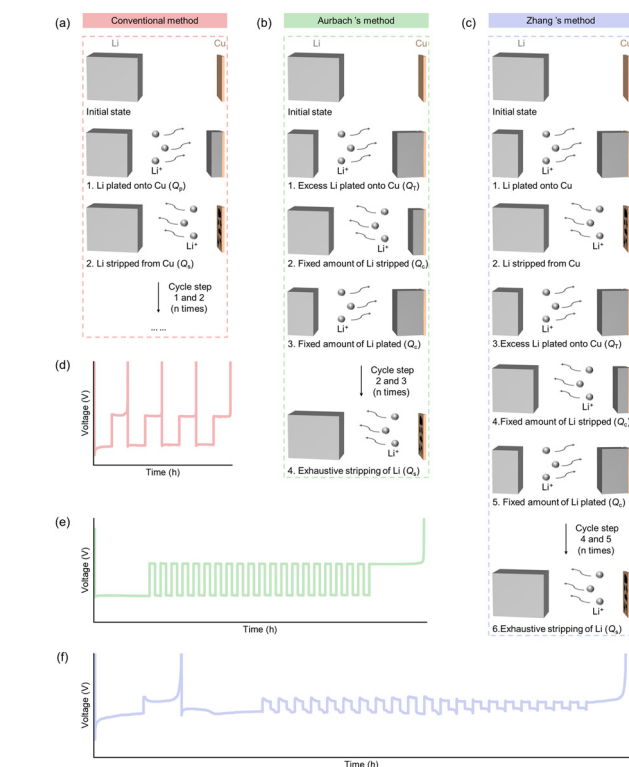

Fig. 3 Schematic diagrams and voltage–time curves of different CE measurement methods. (a) and (d) Conventional methods; (b) and (e) Aurbach's method; (c) and (f) Zhang's method.

cal, as the formation of the SEI is a dynamic process that can significantly impact the CE values obtained in subsequent cycles. Furthermore, the test conditions exert a notable influence on the CE, necessitating careful consideration of various parameters, which include the selection of the substrate, the determination of the stripping cut-off voltage, the choice of cycle numbers, and so forth.[30,75,78,79] These parameters are intricately interwoven within a complex matrix that ultimately dictates the precision and dependability of CE measurements. The intricate and multifaceted interplay among these variables highlights the crucial importance of employing a meticulously crafted experimental design and the implementation of rigorous control protocols.

Reservoir method. To address the stochastic influences imparted by the substrate on CE assessments, Aurbach and co-workers introduced a new testing protocol, colloquially referred to as the "reservoir method" or "Aurbach's method".[80,81] This methodological innovation is predicated on the foundational principle of pre-depositing a surplus of Li metal onto the substrate, thereby establishing a controlled environment for subsequent plating/stripping processes. Consequently, the Li plating and stripping processes are conducted on the surface of Li metal itself, effectively attenuating the influence of substrate on CE quantification.[82,83] A schematic representation of this process is delineated in Fig. 3b and e. In the Aurbach's method, an initial deposition of a sub-

stantial quantity of Li (Q_T) is applied to the Cu substrate, effectively constituting the Li reservoir. Subsequently, a fraction of this reservoir (Q_C) is subjected to n cycles of Li stripping and plating between the working electrode and the counter electrode. Upon completion of these n cycles, the residual Li (Q_S) on the Cu substrate is stripped through the application of an elevated stripping cut-off voltage, a procedure reminiscent of the conventional method. CE is then calculated by employing eqn (3):

$$CE_{avg} = \frac{nQ_C + Q_S}{nQ_C + Q_T}. \tag{3}$$

Aurbach's method is distinguished by its confinement of Li plating and stripping processes to interactions between Li substrates; this serves to minimize the impact of varying substrates and thereby enhances the precision of CE measurements.

However, it is imperative to acknowledge that the initial deposition process is accompanied by the formation and stabilization of the SEI, which inherently leads to the initial capacity loss. Zhang and co-workers posit that the extent of the initial capacity loss during the first cycle is contingent upon the choice of substrate and the methodologies employed for its treatment, accounting for the differences in reported CE across disparate works for identical electrolytes.[75,84] Building upon this insight, Zhang and co-workers refined the primary Aurbach's method by incorporating preliminary SEI formation and a regulation state prior to pre-deposition of the Li reservoir, thereby mitigating the influence of initial capacity loss, as illustrated in Fig. 3c and f. Specifically, prior to the pre-deposition of a reservoir of excess Li, a specific capacity of Li plating/stripping charge (Q_0) is imparted onto the Cu substrate. The magnitude of Q_0 is contingent upon the specific electrolyte employed, and its determination is governed by the following equation:

$$Q_0 = n \times i \times t \tag{4}$$

where n represents the number of cycles necessary for stabilization of the SEI, i denotes the current density utilized during the stabilization process, and t signifies the time required for the SEI to achieve a stable state. Following stabilization of the SEI, subsequent procedures adhere to Aurbach's method, with the calculation of CE being in accordance with eqn (3). This refined method effectively decouples the measurement of CE from the influences of the selection and treatment conditions of the substrate, thereby providing a more accurate reflection of the intrinsic properties of Li metal anodes under specified electrolyte and cycling conditions.

However, it is imperative to recognize that implementation of the reservoir method is inherently more complex and time-consuming compared to the conventional method, which arises from the stringent control required over the amount of Li used in the stabilization process and the pre-deposition process. Meanwhile, a critical consideration in the application of the reservoir method is the substantial pre-deposition of Li

on the Cu substrate, which leads to the capacity of Li metal on the Cu substrate being significantly greater than the capacity of Li metal required in batteries under practical conditions with the limitation of excess capacity of Li metal. The substantial Li reservoir may generate an overestimation of CE, which could obscure the low CE that is likely to arise, given that the available Li capacity is often finite under practical conditions. Consequently, while the reservoir method provides a controlled environment for Li plating and stripping, and offers enhanced accuracy in CE measurements, it is essential to critically assess the impact of a reservoir of excess Li on the results of CE measurements.

2.3.2 Full cells. For full cells, in the first stage, the cathode capacity can be fully discharged due to the presence of surplus Li reservoir on the anode side. Consequently, the CE of full cells is equivalent to the CE of the cathode. In the second stage, the Li reservoir on the anode side is exhausted, and the CE reflects the CE of the anode side. Therefore, the average CE of the anode can be obtained according to capacity retention rates and cycle numbers of full cells.

In the realm of full cells with Li metal anodes, Chiang and co-workers introduced an approximate method for calculating the CE of the anode side in full cells.[59] This method is predicated on the assumption that the CE on the cathode side is 100%, thereby attributing the entire capacity loss of the full cell to the anode side. Consequently, the average CE on the anode side of the full battery can be deduced by monitoring the cycle numbers until its capacity diminishes to 80% of its initial value. The specific equation for this calculation is delineated as follows:

$$\begin{aligned} CE_{avg} &= 1 - \left(\frac{Q_{Li} + 0.2Q_{Cathode}}{n} \right) \times \frac{1}{Q_{Li\,passed\,per\,cycle}} \\ &= 1 - \frac{Q_{Li} + 0.2Q_{Cathode}}{nQ_{Cathode}} \end{aligned} \tag{5}$$

where n denotes the cycle number for the capacity to degrade to 80% of its initial value, and $(Q_{Li} + 0.2Q_{Cathode})/n$ signifies the capacity loss on the anode side per cycle. Consequently, the ratio of $(Q_{Li} + 0.2Q_{Cathode})/n$ to $Q_{Li\,passed\,per\,cycle}$ serves as a basis for calculating the average CE on the anode side. It is important to note that if the capacity does not reach 80% of the initial value within a predefined number of cycles, similar conversion can be executed based on the actual capacity retention rate.

This approach, which leverages the cycle performance of the full cells, allows for a more accurate evaluation of the stability of Li plating/stripping of the Li metal anode under practical conditions compared to the half cells. However, it is important to note that, when the full cells enter the second stage, as mentioned earlier, the capacity of the cathode is gradually unable to be fully discharged. This results in a change in the capacity of each cycle of full cells in the second stage, which in turn means that $Q_{Cathode}$ is no longer a constant in each cycle. This results in an overestimation of CE when calculating the total capacity during the entire lifespan, as the total capacity of

n cycles is less than nQ_{Cathode}. In addition, for a cathode such as NCM, the irreversible phase transition of the cathode occurs in the initial cycle. Consequently, an additional Li reservoir accumulates at the anode, resulting in an underestimation of Li loss throughout the entire lifespan of full cells and, consequently, an inaccurate determination of CE.

Considering these considerations, a modified methodology, which is named Zhang's estimation method, is proposed here. In this approach, the actual total capacity of full cells throughout all n cycles $\left(\sum\limits_{1}^{n} Q_{\text{Charge}}\right)$ is employed in lieu of the theoretical total capacity (nQ_{Cathode}) in the denominator of eqn (5). The total loss of active Li when the capacity decays to 80% retention of the first cycle includes two parts, Q_{Li} and the additional Li reservoir from the cathode, $Q_{\text{Charge (1st)}} - Q_{\text{Discharge (1st)}} + 0.2Q_{\text{Discharge (1st)}} = Q_{\text{Charge (1st)}} - 0.8Q_{\text{Discharge (1st)}}$.

Consequently, eqn (5) can be further modified to give the following equation:

$$CE_{\text{avg}} = 1 - \frac{Q_{\text{Li}} + Q_{\text{Charge (1st)}} - 0.8Q_{\text{Discharge (1st)}}}{\sum\limits_{1}^{n} Q_{\text{Charge}}}. \tag{6}$$

In comparison with the estimation method proposed by Chiang and co-workers, the average CE of the anode can be more accurately estimated by utilizing the actual total capacity of the full cells, as opposed to the theoretical total capacity in Zhang's estimation method. However, it is essential to acknowledge that this assumption of 100% CE for the cathode may lead to an underestimation of the actual CE of the anode. Additionally, it is important to note that this method does not account for the impact of the capacity change resulting from the switching of the charging rate, which also affects the accurate determination of CE. Furthermore, since this method necessitates a significant decline in battery capacity before it can be employed to estimate CE, it demands a relatively extended experimental duration.

Table 1 meticulously delineates the distinct principles, calculation formulas, and comparative merits of various prevalent methods of CE calculation. Within the context of CE computation for various configurations, the imperative selection of an apt method is essential; this facilitates a precise evaluation of the cycling stability of Li metal anodes under practical conditions.

2.4 The brief history of CE improvement

In the domain of early-stage electrolytes, exemplified by ester-based systems, CE is low, with a pronounced tendency to yield substantial quantities of dendritic Li deposits, as delineated in Fig. 4a.[85–88] Under these conditions, the vulnerability of dendritic Li deposits to undergo root fracture during the stripping process precipitates the severance of both electrical and mechanical connections with the anode substrate. This detachment culminates in the genesis of electrically isolated Li^0, which is a significant contributor to irreversible capacity loss. Consequently, at this stage, CE is predominantly influenced by the generation of inactive Li^0, as evidenced in Fig. 4b. The overarching control strategy in this context is to meticulously regulate the deposition behavior of Li, with the aim of diminishing the incidence of dendritic Li deposition, thereby curtailing the production of inactive Li^0 and concurrently enhancing CE.

Upon surpassing a threshold of 95% CE, the deposition morphology of Li metal is observed to be significantly uniform, and the formation of inactive Li^0 is substantially reduced, as graphically represented in Fig. 4a. Concurrently, the CE of the Li metal anode is found to be predominantly influenced by the characteristics of the SEI, as elucidated in Fig. 4c. On one hand, the SEI is often plagued by insufficient stability, making it highly prone to rupture during the processes of Li plating and stripping.[89,90] Therefore, once exposed to the electrolyte due to the compromised integrity of the SEI, the inherently reactive nature of Li metal triggers a series of persistent side reactions. These reactions culminate in the significant conversion of active Li^0 into Li ions within the SEI, contributing to the irreversible loss of capacity. Moreover, the

Table 1 Comparison of various CE calculation methods

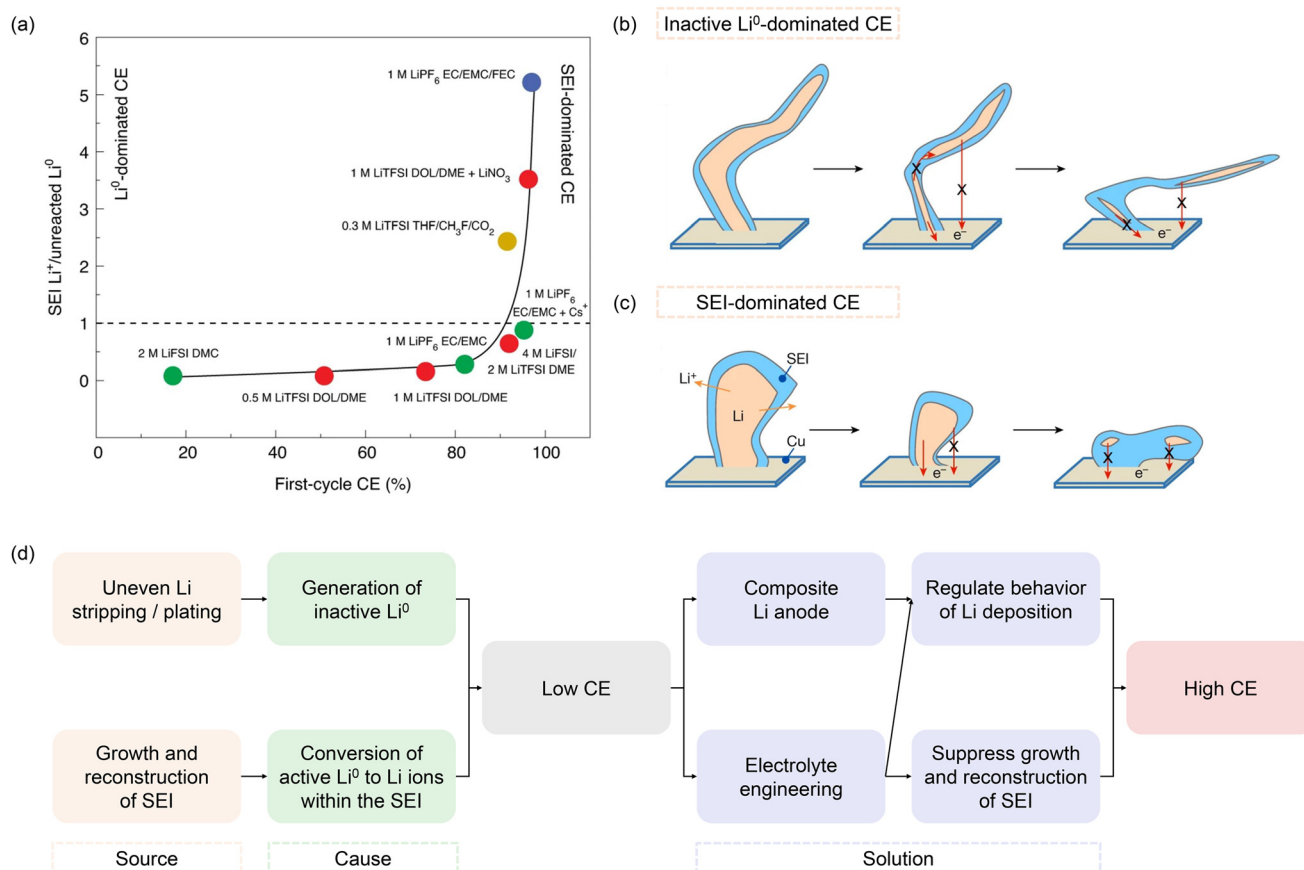| Cell type	Method	Equation	Advantages	Disadvantages
Half cells	Conventional method Aurbach's method	$CE_{\text{avg}} = \dfrac{1}{n}\sum\dfrac{Q_{\text{s}}}{Q_{\text{P}}}$	Simplicity of the procedure	Multitude of interfering factors
	Zhang's method	$CE_{\text{avg}} = \dfrac{nQ_{\text{C}} + Q_{\text{s}}}{nQ_{\text{C}} + Q_{\text{T}}}$	Eliminating the influence of the substrate	Complex testing procedure, overestimation of CE due to excess Li reservoir
Full cells	Chiang's estimation method	$CE_{\text{avg}} = 1 - \dfrac{Q_{\text{Li}} + 0.2Q_{\text{Cathode}}}{nQ_{\text{Cathode}}}$	Reflecting anode cycling stability under practical conditions	Not constant Q_{Cathode}, neglection of irreversible capacity of the cathode
	Zhang's estimation method	$CE_{\text{avg}} = 1 - \dfrac{Q_{\text{Li}} + Q_{\text{Charge (1st)}} - 0.8Q_{\text{Discharge (1st)}}}{\sum\limits_{1}^{n} Q_{\text{Charge}}}$	Considering the change of Q_{Cathode} during cycles and the irreversible capacity of the first cycle	Large workload

Fig. 4 Influencing factors and methods for improving CE in Li metal batteries. (a) Curve of the relationship between the ratio of capacity loss as SEI Li$^+$ to capacity loss as inactive Li^0 to the first-cycle CE[85] (copyright 2021 Springer Nature). Diagram of the effect of inactive Li^0 and SEI Li$^+$ on CE: (b) inactive Li^0-dominated CE and (c) SEI-dominated CE[41] (copyright 2019 Springer Nature). (d) The methods to improve CE for different factors.

conventional SEI in electrolytes exhibits relatively high porosity, and the relentless swelling and dissolving of the SEI result in continuous side reactions between the electrolyte and active Li, leading to capacity loss even in the open-circuit state.[48,49,91] Therefore, it is imperative to address the intrinsic properties of the SEI, including its stability, porosity, and ion and electron transport characteristics, to mitigate these side reactions and furtherly enhance the CE.

2.5 The principles to improve CE

The diminution of active Li on the anode is predominantly ascribed to two interrelated factors: the genesis of Li ions within the SEI, consequent to the growth and construction of the SEI, and the concomitant formation of inert Li^0, attributable to uneven Li plating/stripping. The quest for achieving high-CE Li metal anodes under practical conditions mandates the formulation of strategic interventions that directly confront these underlying issues.

In the realm of enhancing CE in Li metal anodes, composite Li anodes and electrolyte engineering have emerged as the predominant methodologies, as they improve the fundamental issue of Li loss on the anode side, as depicted in Fig. 4d. The composite Li anode involves the incorporation of a host struc-

ture that serves to modulate the deposition kinetics of Li, thereby regulating the behavior of Li deposition and mitigating the proliferation of Li dendrites.[53,92,93] Furthermore, the judiciously engineered host can alter the preferential deposition sites of Li, which in turn diminishes the formation of inert Li^0. Within the domain of electrolyte engineering, the SEI is subjected to precise control through the strategic modification of electrolyte constituents.[94–97] Regulation of the SEI bolsters the uniformity and stability of the SEI, thereby exerting concurrent regulation of the behavior of Li deposition. Moreover, it effectively suppresses the undesired growth and reconstruction of the SEI, thereby optimizing the cycling performance of the Li metal anode. These tailored strategies are instrumental in reducing the irreversible loss of Li at the anode, thereby laying a conducive foundation for the realization of high-CE Li metal anodes under practical conditions.

It is of paramount importance to emphasize that, in the context of practical conditions, rigorous benchmarks must be set for current density and charging capacity. Consequently, in this review, the operational parameters defined as practical conditions include an operating current density that exceeds 1 mA cm^{-2} and a charging capacity that surpasses 3 mAh cm^{-2}. Fig. 5 illustrates recent progress in the improvement of
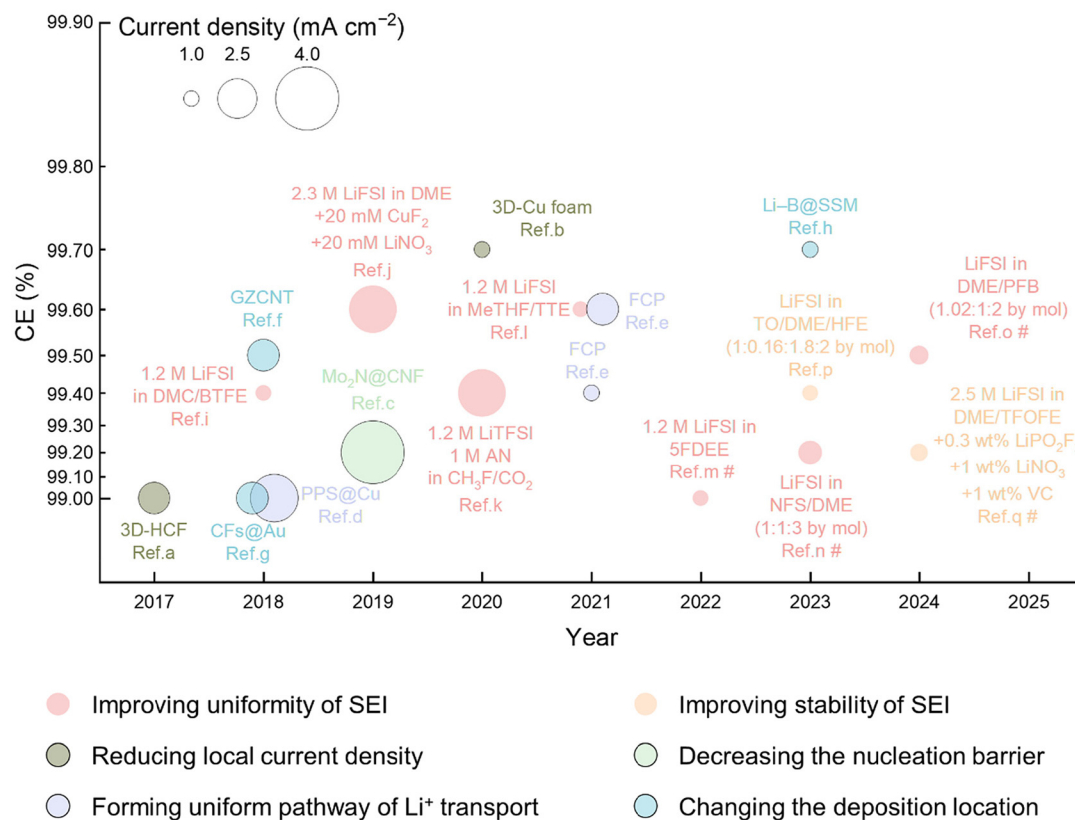
Fig. 5 Advances in high-CE (>99.0%) Li metal anodes under practical conditions in liquid electrolytes. It should be noted that the points counted here are CEs of Li metal anodes measured at a current density of more than 1.0 mA cm^{-2} and a deposition capacity of more than 3.0 mAh cm^{-2}. The points highlighted with black borders represent the strategies for interface engineering, whereas the points without borders indicate strategies for electrolyte engineering. Refs. a–q in this figure correspond to refs. 98–114, respectively. The symbol # denotes that the CE is derived from data for the full cell.

Li metal anodes under practical conditions, which have demonstrated a high CE exceeding 99.0%.[98–114] Table 2 provides a comprehensive summary of the relevant data in Fig. 5. The trajectory of this advancement indicates that, following extensive research and development, the current state-of-the-art CE has not only surpassed the 99.0% threshold but, in some cases, has approached the 99.9% milestone.

However, it is crucial to recognize that the typical service life of contemporary commercial Li-ion batteries extends beyond 5 years, with the ability to maintain stability through over 1500 cycles. This longevity suggests that the average CE of the graphite anode must be no less than 99.95%. Therefore, to effectively compete with graphite and silicon/graphite anodes under practical applications, it is imperative to develop lithium metal anodes with a CE exceeding 99.9%, and ideally surpassing 99.99%, to ensure an extended cycle life under practical conditions. The attainment of elevated CE in the forthcoming period is a matter of significant importance that requires thorough consideration. It is imperative to address this issue to facilitate the practical application and commercial viability of Li metal anodes, as it has a direct impact on their performance and lifespan in practical energy storage systems.

3   Advances in high-CE Li metal anodes under practical conditions

3.1   Composite Li anodes

Composite Li anodes are engineered with a robust three-dimensional (3D) host that capitalizes on its high specific surface area and adjustable characteristics to effectively manage Li plating and stripping processes. This section aims to dissect the core principles and operational dynamics of these composite anodes, highlighting the significant progress made in developing high-CE Li metal anodes suitable for practical applications.

3.1.1   The principles of composite Li anodes. The initial conception of the composite Li anode was predicated on the utilization of its 3D structure to furnish ample space for Li deposition, thereby mitigating the volumetric perturbations engendered by Li plating and circumventing the rupture of the SEI.[115–118] With the evolution of a deeper understanding of the host, researchers have progressively shifted their focus towards elucidating the underlying mechanisms governing Li dendrite growth. Among a myriad of models proposed, the space charge

Table 2 Summary of the advances in high-CE (>99.0%) Li metal anodes under practical conditions in liquid electrolytes

Method	Mechanism	Year	Materials/electrolytes	Current density (mA cm^{-2})	CE (%)	Ref.
Composite Li anodes	Reducing local current density	2017	3D HCF	2.0	99.0 (half cell)	98
		2020	3D Cu	2.0	99.7 (half cell)	99
	Decreasing the nucleation barrier	2019	Mo$_2$N@CNF	4.0	99.2 (half cell)	100
	Forming uniform pathway for Li$^+$ transport	2018	PPS@Cu	3.0	99.0 (half cell)	101
		2021	FCP	1.0	99.4 (half cell)	102
	Changing the deposition location	2018	GZCNT	2.0	99.6 (half cell)	103
		2018	CFs@Au	2.0	99.5 (half cell)	104
		2023	Li-B@SSM	2.0	99.0 (half cell)	105
Electrolyte engineering	Improving uniformity of the SEI	2018	1.2 M LiFSI in DMC/BTFE	1.0	99.7 (half cell)	106
		2019	2.3 M LiFSI in DME + 20 mM CuF$_2$ + 20 mM LiNO$_3$	3.0	99.6 (half cell)	107
		2020	1.2 M LiTFSI, 1 M AN in CH$_3$F/CO$_2$	3.0	99.4 (half cell)	108
		2021	1.2 M LiFSI in MeTHF/TTE	1.0	99.6 (half cell)	109
		2022	1.2 M LiFSI in 5FDEE	1.0	99.0 (full cell)	110
	Improving stability of the SEI	2023	LiFSI in NFS/DME (1:1:3 by mol)	1.5	99.2 (full cell)	111
		2024	LiFSI in DME/PFB (1.02:1:2 by mol)	1.2	99.5 (full cell)	112
		2023	LiFSI in TO/DME/HFE (1:0.16:1.8:2 by mol)	1.0	99.4 (full cell)	113
		2024	2.5 M LiFSI in DME/TFOFE + 0.3 wt% LiPO$_2$F$_2$ + 1 wt% LiNO$_3$ + 1 wt% VC	1.1	99.2 (full cell)	114

model, articulated by Chazalviel and colleagues, has garnered widespread acceptance.[119] This model posits that dendritic growth is produced by the presence of a space charge layer within the electrolyte of low concentration. As the concentration of Li ions at the surface of the anode asymptotically approaches zero in concert with escalating current density, the nucleation and proliferation of dendrites are incited. This phenomenon, denoted as Sand's behavior, is characterized by a critical temporal threshold, termed Sand's time (τ), which is delineated by the ensuing equation:

$$\tau = \pi D \frac{e^2 C_0{}^2 (\mu_a + \mu_{Li^+})^2}{(2J\mu_a)^2} \qquad (7)$$

where μ_a, μ_{Li^+}, C_0 and J correspond to the mobilities of anions and Li ions, the initial concentration of Li ions, and the current density, respectively. The term D signifies the ambipolar diffusion coefficient, which is a composite parameter that is related to the diffusion coefficients and mobilities of both Li ions and anions. Consequently, it can be deduced that Sand's time, which is a critical parameter in the context of Li dendrite formation, can be significantly prolonged by effectively diminishing the local current density. This extension of Sand's time is instrumental in curbing the proliferation of Li dendrites, thereby enhancing the overall stability and reliability of Li metal anodes.

Beyond the effects of space charge, the proliferation of Li dendrites is further modulated by the properties of the substrate and the SEI.[23,120–122] The substrate exerts a pivotal influence on the nucleation barrier and the rate of Li deposition, which are critical factors in determining the initial stages of Li dendrite formation. Additionally, the SEI plays a significant role in dictating the uniformity of Li ion distribution across the anode/electrolyte interface, thereby impacting the uniformity of Li deposition. Moreover, the unique structure of the host can alter the preferential sites for Li deposition, thereby ameliorating the deposition behavior of Li. This structural modification is instrumental in mitigating the deleterious effects of dendrite growth on the cycle performance of the anode.

In summary, the core concept of the composite Li anode design is rooted in the strategic incorporation of a 3D scaffold, complemented by intentional modification techniques, to significantly reduce the growth of Li dendrites and simultaneously improve the CE of Li metal anodes under practical operating conditions.

3.1.2 Suppressing Li dendrites

Reducing local current density. In accordance with the Sand's time model, a reduction in local current density is a pivotal strategy for mitigating the growth of Li dendrites. Consequently, the fundamental role of the composite Li anode is to diminish local current density by leveraging its distinctive 3D structure, which endows it with a substantial specific surface area, as depicted in Fig. 6a. Furthermore, the intrinsic porous structure of the composite Li anode offers a substantial volume to accommodate the deformation associated with Li deposition.
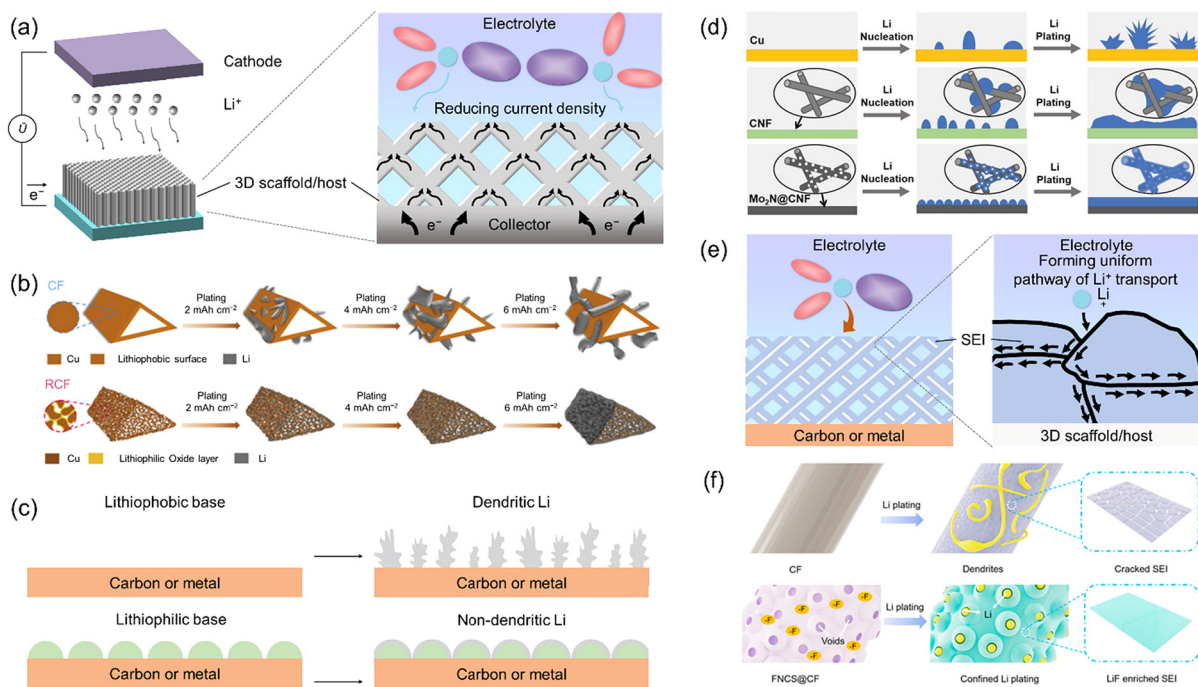
Fig. 6 Reducing the formation of dendritic Li deposition by composite Li anodes. (a) Schematic diagram and (b) the application of a 3D host to reduce local current density[99] (copyright 2020 Elsevier). (c) Schematic diagram and (d) the application of a modified lithiophilic host to decrease the nucleation barrier[100] (copyright 2019 Wiley-VCH). (e) Schematic diagram and (f) the application of a modified host to form a uniform pathway of Li ions[102] (copyright 2021 American Chemical Society).

The carbon host, renowned for its low density, high electrical conductivity, and exceptional chemical stability, is a prevalent component in the construction of composite Li anodes.[123–129] Guo and co-workers demonstrated the utilization of 3D hollow carbon fibers (3D-HCF), which possess a high conductive active surface area, to achieve a CE of about 99.0% over 90 cycles at a current density of 2 mA cm^{-2} and a deposition capacity of 4 mAh cm^{-2}.[98] However, it is crucial to recognize that carbon, in its native state, demonstrates a relatively low affinity for Li metal, which inherently limits the behavior of Li deposition.[130,131] Concurrently, the increased specific surface area of carbon makes it more susceptible to catalyzing enhanced side reactions with the electrolyte, which can potentially compromise the stability of the anode.[132,133] As a result, the application of pure carbon as a host material in anode research and development is gradually declining.

The strategic design and preparation of conventional materials of a collector, such as Cu, Ni, and stainless steel, in a 3D structure have been demonstrated to effectively mitigate the proliferation of Li dendrites.[134–136] This approach leverages the intrinsic benefits of metal materials, including high electrical conductivity, superior mechanical and chemical stability, and cost-effectiveness. Li and colleagues successfully engineered a rimous copper foam (RCF) with an ant-nest-like porous structure through an innovative polysulfide-assisted reconstruction technique, as depicted in Fig. 6b.[99] As a result, the composite Li anode, when integrated with RCF, demonstrates

an exceptional CE of 99.7% across 180 cycles at a current density of 1 mA cm^{-2} and a deposition capacity of 4 mAh cm^{-2}. However, the high density of the metal-based host results in a significant reduction in the specific capacity of composite Li anodes, which is detrimental to the enhancement of the energy density of Li metal batteries.[137,138] Therefore, the future development of high specific capacity and light weight metal-based composite Li anodes represents a critical focus that warrants consideration in the ongoing pursuit of advanced high-CE Li metal anodes.

Decreasing the nucleation barrier. While 3D materials can serve as the hosts of composite Li anodes, the potential surface inhomogeneities may lead to non-uniform current distribution, culminating in uneven Li deposition. In seminal work published in 2016, Cui and co-workers proposed the concept of "lithiophilic" materials.[139] According to the heterogeneous nucleation model, the nucleation overpotential for Li metal on certain substrates is negligible or minimal, suggesting an exceptional affinity between these materials and Li metal, which is defined as lithiophilicity, as shown in Fig. 6c. This lithiophilicity arises from the ability of these substrates to react with Li prior to the formation of a distinct phase of Li metal, yielding a solid solution with a crystallographic structure akin to that of Li metal. Acting as an intermediary layer for subsequent Li deposition, this solid solution significantly diminishes the nucleation barrier, thereby facilitating the uniform deposition of Li and enhancing the cycling performance of the anode.

Generally, metal elements capable of forming alloys with Li, such as tin (Sn), silver (Ag), zinc (Zn), magnesium (Mg), and others, exhibit lithiophilicity.[140–142] These metal elements can be strategically doped into the hosts to serve as lithiophilic sites, thereby decreasing the Li nucleation barrier.[139,143] Gong and co-workers employed a Ag-modified Cu collector as a lithiophilic host to prepare a composite Li anode, which achieved over 120 cycles with a CE exceeding 98.8% at a current density of 1 mA cm^{-2} and a deposition capacity of 3 mAh cm^{-2}.[144] Beyond metallic elements, certain non-metallic elements, including oxygen (O), nitrogen (N), sulfur (S), and others, are recognized for their lithiophilicity.[145–147] This characteristic is ascribed to their ability to serve as Lewis base sites, a function that arises from their significant electronegativity and the availability of lone pair electrons. These attributes empower these non-metallic elements to efficiently adsorb Li ions, which, in turn, act as a Lewis acid.

Besides single-element modification, some compounds, including metal oxides and metal nitrides, have been identified to exhibit lithiophilicity.[148–151] In these compounds, both O and N exhibit elevated electron densities, which endow them with the propensity to form strong interactions with Li. Moreover, these compounds can engage in redox reactions with Li, yielding products such as lithium oxide (Li_2O) and lithium nitride (Li_3N) that possess high Li ion conductivity, resulting in facilitating the expeditious diffusion of Li ions. Manthiram and co-workers engineered a composite Li anode by employing a straightforward modification of Mo_2N on the surface of carbon nanofibers, as depicted in Fig. 6d.[100] The high lithiophilicity of Mo_2N has been instrumental in endowing the composite Li anode with remarkable stability, as demonstrated by its ability to undergo 150 cycles with an average CE up to 99.2% at a current density of 4 mA cm^{-2} and a deposition capacity of 3 mAh cm^{-2}.

It is essential to acknowledge that the beneficial effects of lithiophilic surface modifications may be concealed and neutralized by the presence of "dead Li", which includes non-functional Li and the SEI, more so under practical conditions.[152] Therefore, a pivotal strategy for improving CE lies in the targeted reactivation of "dead Li" on the surface of the host, thereby reigniting the lithiophilic sites.

Forming a uniform pathway for Li ions. The migration of Li ions across the surface of the anode is a pivotal factor influencing the deposition morphology of Li metal.[153,154] The uniformity of Li ion distribution at the anode/electrolyte interface is directly correlated with the deposition rate of Li, which in turn dictates the plating morphology of Li metal. Forming a uniform pathway for Li ion transport on the surface of composite Li anodes is an efficacious strategy to mitigate the proliferation of Li dendrites.[73,155,156]

Surface modification of composite Li anodes through the engineering of the SEI is a prevalent strategy for establishing uniform pathways for Li ion transport.[157,158] The incorporation of inorganic constituents, such as lithium fluoride (LiF) and Li_3N, into the SEI has been demonstrated to significantly enhance both the rate and uniformity of Li ion transport, fostering a uniform Li deposition morphology. Li and co-workers developed a composite Li anode featuring a LiF-rich SEI layer by subjecting a carbon fiber host to fluorination, as depicted in Fig. 6f.[102] This composite Li metal with LiF-rich SEI modification maintains a high CE of 99.4% over 150 cycles at a current density of 1 mA cm^{-2} and a deposition capacity of 4 mAh cm^{-2}, and an even higher CE of 99.6% over 200 cycles at a current density of 2 mA cm^{-2} and a deposition capacity of 3 mAh cm^{-2}.

Polymeric materials are frequently employed in the construction of composite Li anodes, leveraging their enriched polar functional groups on the surface, such as the cyanide group (–CN) and hydroxyl group (–OH), to facilitate interactions with Li ions and thereby establish a uniform Li ion transport pathway.[159–162] Wang and co-workers reported the utilization of a 3D cross-linked porous polyethylenimine sponge (PPS) as a host for the composite Li anode, which exhibited pronounced affinity for Li ions, due to its polar functional groups.[101] Consequently, the composite Li anode with PPS host achieves a high CE of 99.0% over more than 450 cycles at a current density of 3 mA cm^{-2} and a deposition capacity of 4 mAh cm^{-2}.

3.1.3 Changing the location of Li deposition. During periods of high rates of Li deposition, Li tends to preferentially deposit at the top of the host, a phenomenon referred to as "top-growth", as illustrated in Fig. 7a.[163,164] This behavior arises from the propensity for a concentration gradient to form between the electrolyte and the anode in the battery. The concentration of Li ions is elevated at the top of the host near the electrolyte side and diminishes progressively in the vertical direction towards the bottom of the host. Consequently, Li is more readily deposited at the top of the composite Li anode, which results in suboptimal spatial utilization and impedes the efficient deposition of Li throughout the entire host structure.

To address the challenge, Mai and co-workers introduced the innovative concept of a gradient host in 2018, as depicted in Fig. 7c.[103] The bottom layer of the host is composed of carbon nanotubes (CNT) loaded with lithiophilic zinc oxide (ZnO), while the top layer of the host retains the original lithiophobic CNT substrate. With this configuration of lithiophilic–lithiophobic gradient host, in which Li preferentially deposits at the bottom of the host, the spatial utilization of the host is enhanced, as demonstrated in Fig. 7b. The structural design of the composite Li anode with a gradient skeleton structure not only changes the location of Li deposition but also significantly improves the cycling performance. Specifically, the anode can be stabilized for 100 cycles, achieving an average CE of up to 99.5% at a current density of 2 mA cm^{-2} and a deposition capacity of 3 mAh cm^{-2}. In addition to the development of a gradient lithiophilicity host, various other gradient host designs have been conceived with analogous objectives to change the location of Li deposition, such as electrical conductivity and pore size.[165,166] Beyond the gradient host, a range of meticulously designed hosts with specialized structures have been implemented to control the site of Li deposition.[104,105]

In the realm of enhancing the CE of Li metal anodes under practical conditions, the employment of composite Li anodes
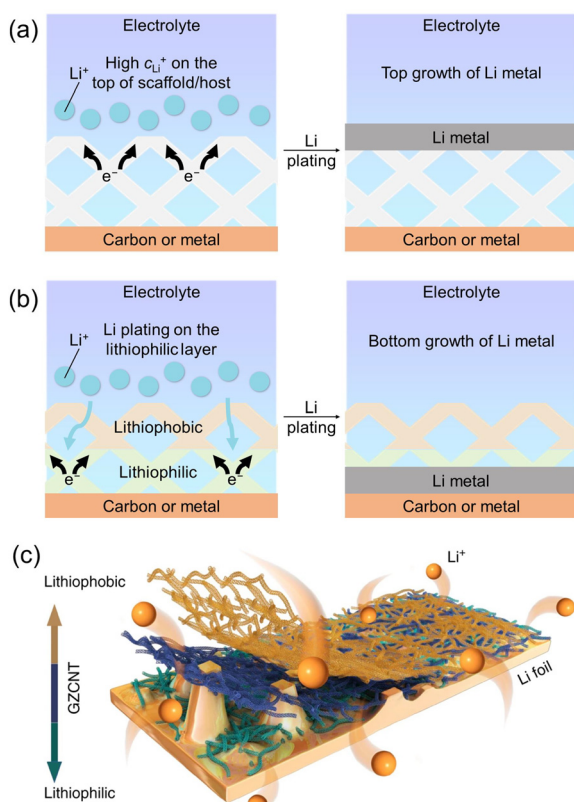
Fig. 7 Changing the location of Li metal deposition by gradient composite Li anodes. Schematic diagram of Li deposition location of (a) normal host and (b) gradient host. (c) Application of a lithiophilicity-gradient host[103] (copyright 2018 Springer Nature).

has indeed witnessed significant advancements. However, the incorporation of a host within composite Li anodes results in an increase in the overall mass and volume of the anode, reducing the energy density of Li metal batteries, which is a critical parameter for meeting the high-energy-density requirements of practical applications. Consequently, the future trajectory of research and development in composite Li anodes must prioritize the creation and optimization of light weight hosts. Such innovations are essential to align with the practical deployment of Li metal batteries, ensuring that they can deliver on the advantage of high energy density while maintaining stability and safety for commercialization.

3.2 Electrolyte engineering

The electrolyte plays a pivotal role in Li metal batteries. Modulating the composition and concentration of the electrolyte can directly influence the SEI, thereby improving the CE of Li metal anodes. This section primarily delineates the design principles of electrolyte engineering and the underlying logic for controlling the SEI, particularly emphasizing the improvement of the uniformity and stability of the SEI, with a focus on research advancements in the field of high-CE Li metal anodes under practical conditions.

3.2.1 The principles of electrolyte engineering. The concept of electrolyte engineering was initially proposed to

address the instability issues associated with Li metal anodes. Due to the extremely low electrode potential and high chemical reactivity of Li metal, it readily reacts with electrolyte components to form the SEI.[167–169] The properties of the SEI, such as uneven Li ion transport and the mechanical instability of the structure, can lead to non-uniform Li plating/stripping, accompanied by the growth of Li dendrites and the generation of a significant amount of inactive Li.[170,171] Therefore, to solve the instability problems of Li metal anodes, it is essential to reconcile the conflict between Li metal and electrolyte. The formation of the SEI with a uniform chemical composition and robust mechanical structure, achieved through the regulation of the electrolyte, is anticipated to facilitate uniform Li growth at the source and prevent the continuous rupture and reconstruction of the SEI, thereby markedly enhancing the cycling reversibility and safety of Li metal anodes. Thus, electrolyte engineering is defined as the process of optimizing the composition and structure of the electrolyte to improve the properties of the SEI, ultimately aiming to enhance the cycling performance of Li metal anodes.

From a temporal perspective, as illustrated in Fig. 4d, the low CE of Li metal anodes originated from non-uniform Li plating/stripping and the continuous growth and reconstruction of the SEI. During the nascent phase of cycling, Li ions ensconced within electrolyte solvation shells are directed towards the anode. Upon reaching the anode surface, these electrolytes undergo reduction and concurrent decomposition, culminating in the formation of a nascent SEI. The uniformity of Li-ion transport through the SEI at this stage directly affects the plating/stripping process of Li metal.[172] Non-uniform Li plating and stripping can result in the accumulation of a substantial quantity of inactive Li. In addition, volume changes in the Li metal anodes during repeated cycles are inevitable; the SEI is fragile and undergoes cracking and reconstruction.[76] Furthermore, due to the dissolution of the SEI, the electrolyte permeates into the SEI and continuously undergoes reduction reactions with Li metal, leading to further loss of active Li and a decrease in the CE of the anode. Therefore, the uniformity, mechanical stability, and passivation capability of the SEI are crucial for enhancing the CE of Li metal anodes. In the following section, pragmatic approaches to improving the CE of Li metal anodes through three facets of electrolyte optimization are discussed: improving uniformity, improving the mechanical and chemical stability of the SEI, and other aspects.

3.2.2 Improving the uniformity of the SEI. The SEI, composed of inorganic and organic components, covers the surface of Li metal and serves to insulate electrons and conduct ions. Consequently, the ion transport rate and the uniformity of ion transport within the SEI directly determine the uniformity of Li deposition during charging, which in turn affects the cycling stability of the Li metal anode. It is generally believed that an SEI rich in inorganic components is conducive to improving the uniformity of Li-ion transport, and achieving uniform Li nucleation and growth.[24,173–175] Inorganic components such as LiF, Li_3N, and Li_2O, exhibit a polycrystalline domain mosaic structure within the SEI, featur-

ing abundant grain boundaries.[176] The energy barrier for Li-ion diffusion through grain boundaries is lower, resulting in faster transport rates. At the same time, taking into account the differences in atomic configuration and surface imperfections, the Li atom shows a tendency to adsorb on inorganic surfaces with higher surface energy, thus facilitating its transversal diffusion and consequently impeding the proliferation of vertical dendrites.[177]

The composition of Li ions in the solvation structure preferentially participates in reduction and decomposition, forming the SEI. By regulating the solvation structure of Li ions, the raw materials for SEI formation can be altered, thereby controlling the composition of the SEI. As shown in Fig. 8a, in conventional electrolytes, solvent molecules are reduced at the surface of Li metal to form an SEI rich in organic components. Due to the non-uniformity of Li ion flux, the SEI formed exacerbates the unevenness of the anode/electrolyte interface. Anions such as the bis(fluorosulfonyl)imide anion (FSI^-) can produce inorganic components like LiF and Li_3N, which can promote Li ion transport within the SEI and are widely used in electrolyte engineering. The increase in coordination of anions with Li ions lowers the energy level of the lowest unoccupied molecular orbital (LUMO) of anions, leading to increased reactivity and preferential reduction of anions over solvents, resulting in an anion-derived SEI.[178–180] In 2015, Qian et al. first used a high-concentration electrolyte (HCE) composed of 4 M LiFSI in dimethoxyethane (DME), achieving stable cycling and a high average CE for Li metal anodes.[181] The interaction of Li ions with anions and solvents is enhanced at high electrolyte concentrations, resulting in anions entering the solvation shell

of Li ions to balance the excess positive charge of Li ions. At this juncture, the quantity of free solvent molecules is diminished, and the proportion of contact ion pairs and aggregates is augmented. Considering the high viscosity of HCE and the cost issues associated with high Li salt concentrations, Chen et al. introduced BTFE as a diluent, replacing the original dimethyl carbonate (DMC) solvent, forming a localized high-concentration electrolyte (LHCE) without affecting the participation of anions in the solvation structure of Li ions.[106] The assembled Li|Cu cells exhibited an average CE of 99.4% at a current density of 1 mA cm^{-2} and a deposition capacity of 5 mAh cm^{-2}. As shown in Fig. 8b, Xu et al. demonstrated that by tuning strong anion–cation coordination structures in a compatible low-polarity solvent and employing a nucleation modulation procedure, the Li plating/stripping process exhibited an impressive average CE of 99.6% under rather demanding conditions (a current density of 1 mA cm^{-2} and a deposition capacity of 3 mAh cm^{-2}).[109] Yao et al. proposed a weakly solvating electrolyte comprised of nonpolar pure solvents with the objective of achieving anion-dominated interfacial chemistry.[182] In contrast to LHCE, no diluent is postulated in WSE, and some of the weakly solvated solvents are engaged in the solvation process, thereby enhancing ionic conductivity. Recent research in the field of electrolyte engineering has been burgeoning, with numerous novel insights being proposed to design specialized electrolyte solvation structures. Jie et al. revealed the formation of a large and compact ion-pair aggregate (CIPA) electrolyte with short Li^+–Li^+ distances (Fig. 8c), which promoted fast interfacial reduction kinetics via a collective electron-transfer mechanism, forming a stable and thin
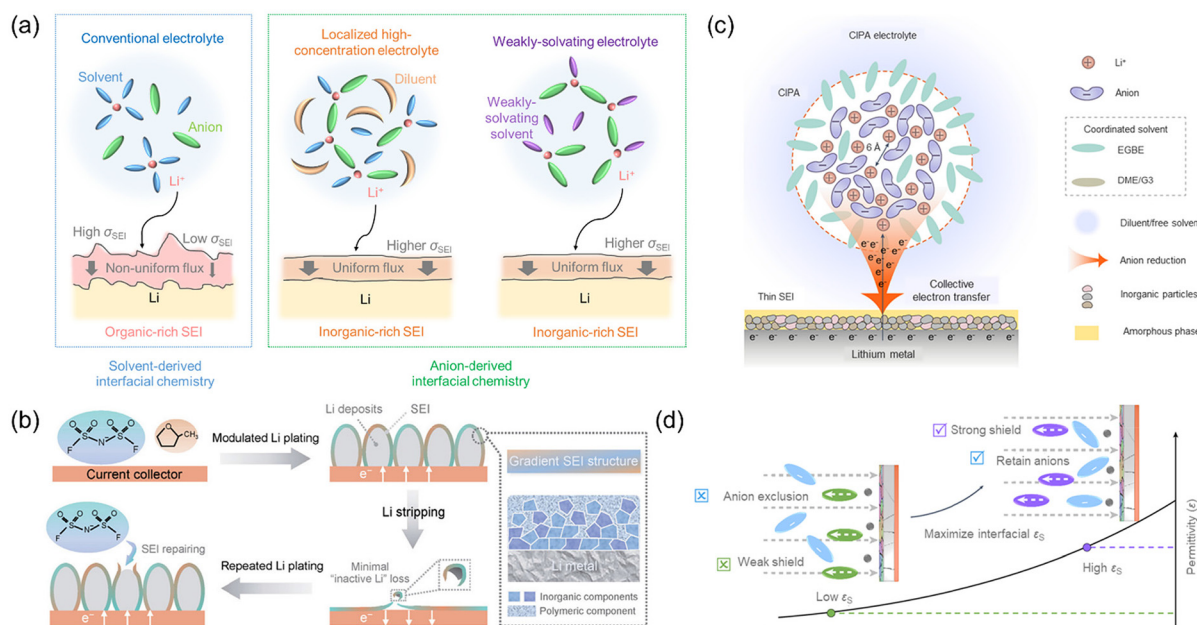

Fig. 8 Improving SEI uniformity by regulating the solvation structure in electrolytes. (a) Schematic diagram of the solvation structure and the corresponding SEI in different electrolytes. Application of regulating the solvation structure in electrolytes: (b) localized-high-concentration electrolyte[109] (copyright 2021 Wiley-VCH), (c) compact ion-pair aggregate (CIPA) electrolyte[183] (copyright 2024 Springer Nature). (d) Tuning interfacial dielectric environment to reform the ionic distribution[112] (copyright 2024 Springer Nature).

SEI with a low organic content.[183] As shown in Fig. 8d, Zhang *et al.* explored the interfacial electric field and its impact on cation solvation and SEI formation. 1,1,1,3,3-Pentafluorobutane (PFB) is chosen to refine a high dielectric environment preserving the integrity of cation–anion coordination and promoting the formation of an anion-derived SEI.[112] This research demonstrates the feasibility of this protocol with a 6 Ah Li metal pouch cell achieving an energy density of 500 Wh kg^{-1} using an ultra-lean electrolyte.

In addition to optimizing the composition of salts and solvents, functional additives serve as another effective approach for significantly enhancing the CE of Li metal anodes. As depicted in Fig. 9a, additives generally exhibit higher reactivity than the original components of the electrolyte and can react and decompose with Li metal prior to the salts or solvents, obtaining an SEI with specific components and structure.[184] Theoretical analysis results from first-principles and *ab initio* molecular dynamics indicate that ethylene carbonate fluoride (FEC) can decompose preferentially over ethylene carbonate (EC) and diethyl carbonate (DEC), generating LiF. As shown in Fig. 9b, Zhang *et al.* experimentally confirmed that the introduction of FEC as an additive in Li metal batteries could significantly enhance the CE and lifespan of the full cell.[185] Lithium nitrate (LiNO$_3$), as one of the most effective additives, has been widely studied and used. The decomposition of NO$_3^-$ leads to the formation of a multi-layered SEI rich in Li$_3$N and Li$_2$O, promoting the growth of spherical Li nucleation and the uniform deposition of Li metal.[186] Due to the poor solubility of LiNO$_3$ in carbonate esters, Yan *et al.* introduced trace amounts of CuF$_2$ as a dissolution promoter, allowing LiNO$_3$ to be directly dissolved in EC/DEC electrolytes (Fig. 9c).[107] At a current density of 3 mA cm^{-2} and a charging capacity of 3 mAh cm^{-2}, Li|Cu half cells were stable for 150 cycles with an average CE of 99.6%. Organic nitrates, such as isosorbide dini-

trate (ISDN) molecules with organic groups that are compatible with esters, can notably improve the uniformity of the SEI as an alternative to LiNO$_3$.[187] As illustrated in Fig. 9d, Zhang *et al.* demonstrated the formation of a bilayer SEI using ISDN additives in localized high-concentration electrolytes.[188] The performance of Li|LiNi$_{0.5}$Co$_{0.2}$Mn$_{0.3}$O$_2$ (NCM523) batteries under practical conditions achieves 625 cycles based on 80% capacity retention. In addition, Kim *et al.* investigated that the addition of 7 wt% Li$_2$O nanoparticles to liquid electrolytes modified the Li-ion solvation environment, reducing the Li nucleation overpotential, leading to an inorganic-rich SEI with improved electrochemical performance, as shown in Fig. 9e.[189]

3.2.3 Improving the mechanical and chemical stability of the SEI.
The formation of Li dendrites and the constant rupture and repair of the SEI have resulted in a significant depletion of the active Li reserves, leading to a decline in battery capacity and impeding the advancement of lithium metal batteries. The composition and structure of the SEI significantly influence its mechanical properties and determine its ability to withstand stress and strain. An ideal SEI should possess a large elastic strain limit, resisting significant volumetric deformation, and be sufficiently robust to maintain itself without fracturing.[95,190] Selecting or designing an SEI that can form with high toughness is crucial for better withstanding the mechanical stresses generated during Li dendrite growth, thereby reducing dendrite penetration. Early research indeed indicated that inorganic components played a role in enhancing the Young's modulus of the SEI. As understanding has deepened, attention has also turned to the synergistic effects of organic and inorganic components within the SEI.[191] In 2017, utilizing sulfur-containing polymers (SCPs) as electrolyte additives was proposed to form a flexible hybrid SEI through the co-deposition of organosulfides/organopolysulfides and inorganic salts.[192] As depicted in Fig. 10a, the
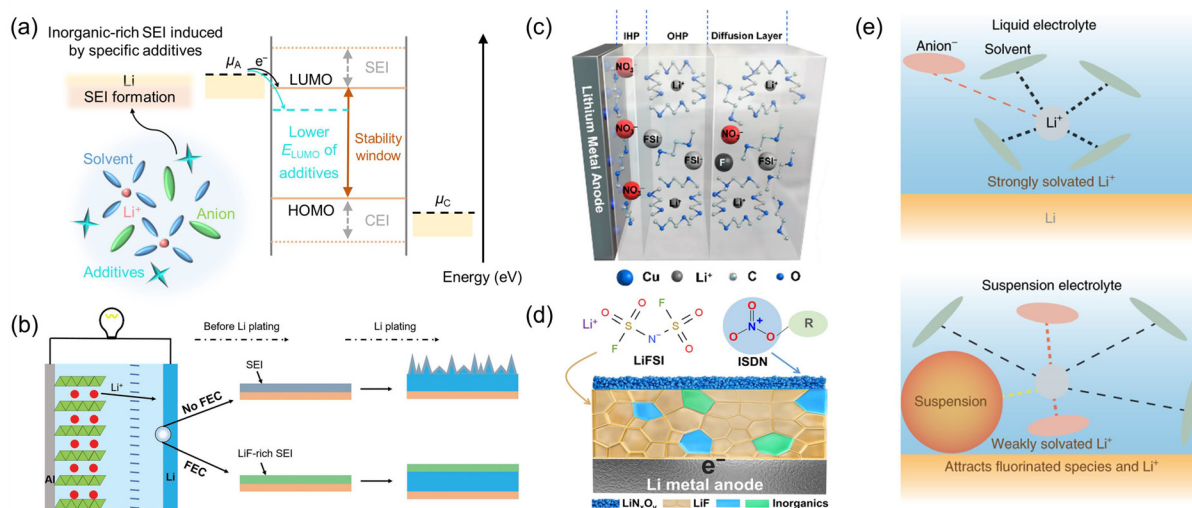

Fig. 9 Improving SEI uniformity by introducing additives to form an SEI with specific components. (a) Schematic diagram of the working mechanism of additives in forming the SEI. Application of specific additives: (b) FEC[185] (copyright 2017 Wiley-VCH), (c) LiNO$_3$[107] (copyright 2019 American Chemical Society), (d) ISDN[188] (copyright 2023 Wiley-VCH), and (e) Li$_2$O particles[189] (copyright 2022 Springer Nature).
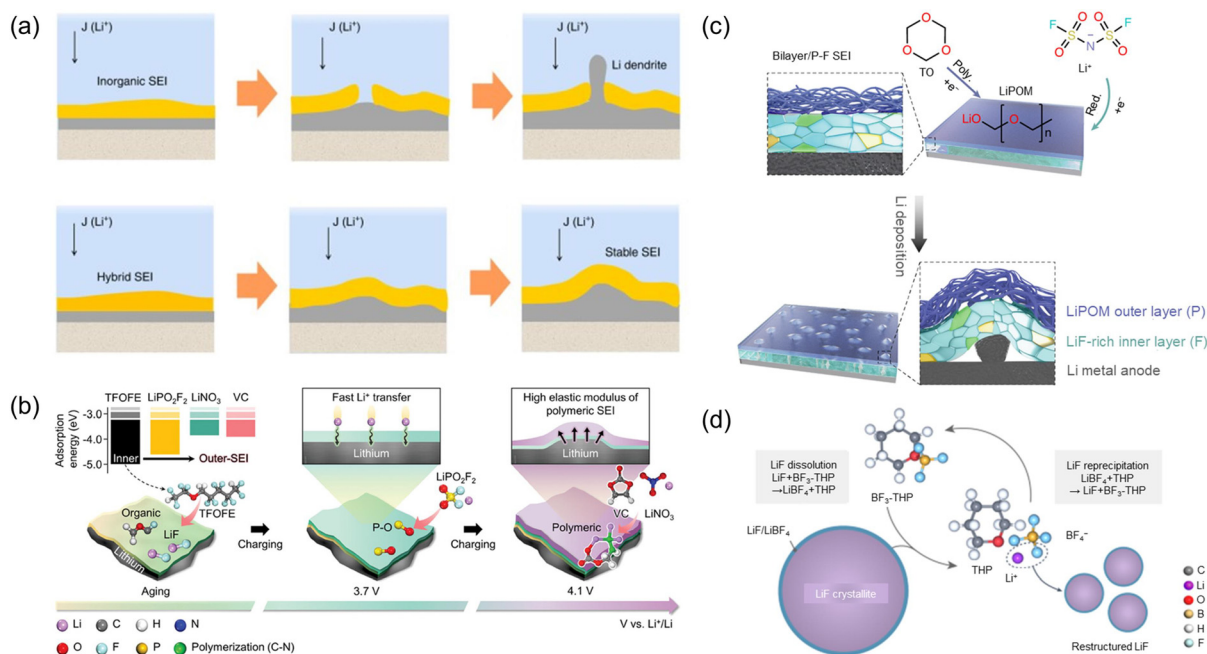
Fig. 10 Strategies to improve the mechanical stability and chemical stability of the SEI. (a) Inorganic/organic hybrid SEI layer formed by sulfur-containing polymer additives. (b) The sequenced multilayer SEI formed by LiPO$_2$F$_2$, LiNO$_3$, and VC additives[114] (copyright 2024 Wiley-VCH). (c) Bilayer/P–F SEI generated by trioxane−modulated electrolyte[113] (copyright 2023 Springer Nature). (d) Restructuring of LiF crystallites suppressing Li corrosion *via* borate−pyran electrolyte[196] (copyright 2024 Springer Nature).

organic polysulfides formed from the decomposition of additives acted as "plasticizers", enhancing the flexibility of the SEI, while the inorganic components provided Li-ion conduction pathways and the necessary mechanical hardness. Thus, the arrangement of various components is crucial to regulate the homogeneity and mechanical stability.[193,194] As shown in Fig. 10c, Zhang *et al.* demonstrated that the bilayer structure constructed *in situ* in trioxane (TO)-modulated electrolyte featured an inner layer that was LiF-rich, which homogenized Li-ion fluxes, and an outer layer with Li polyoxymethylene (LiPOM) to enhance mechanical stability.[113] As depicted in Fig. 10b, Lee *et al.* enriched research on a multilayer SEI synthesized by the sequential reduction of 1,1,2,2-tetrafluoroethyl-1*H*,1*H*,5*H*-octafluoropentyl-ether (TFOFE), Li difluorophosphate (LiPO$_2$F$_2$), LiNO$_3$, and vinylene carbonate (VC).[114] The LiF-rich inner SEI derived from TFOFE offers electronic insulation, high mechanical strength, and broad electrochemical stability. Meanwhile, the organic-species-containing inner layer and P–O-species-based middle layer, which facilitate Li-ion transport across the SEI, together with the polymeric outer layer, formed from VC and LiNO$_3$ during Li plating/stripping, strengthen the mechanical integrity of the SEI.

In addition to the methods previously discussed to enhance the mechanical stability of the SEI, improving the chemical stability of the SEI is equally important. Chemical corrosion occurs at the defects of the SEI, where active components in the electrolyte react further with the SEI, leading to its decomposition and the release of corrosive substances, which result in a decline in battery performance. Electrochemical cor-

rosion refers to the oxidation–reduction reactions that occur in the SEI during electrochemical processes, causing its decomposition and the corrosion of electrode materials.[195] In 2018, Li *et al.* investigated the impact of SEI component distribution on its structural stability. It was found that in the mosaic SEI formed in standard carbonate-based electrolytes, rapid Li dissolution occurred in local areas with high grain concentration, leading to the collapse of the SEI structure and the formation of inactive Li. In contrast, in the multi-layered SEI formed in an EC/DEC electrolyte with the addition of 10 vol% FEC, the distribution of organic and inorganic components is uniform, and Li deposition behavior is more uniform.[194] As shown in Fig. 10d, Kwon *et al.* proposed that an electrolyte based on borate–pyran could transform large LiF microcrystals in the SEI into fine crystals or glassy states, achieving the reorganization of LiF crystals and minimizing further penetration of the electrolyte into the SEI, thereby enhancing the passivation capability of the SEI.[196] In addition, galvanic corrosion cannot be ignored due to the presence of metal current collectors or battery casings. The oxidation dissolution of Li and the reduction decomposition of the electrolyte usually occur at the interface where Li is in contact with the Cu current collector.[195,197] Developing strategies for current collector passivation with good electrical insulation and low electrolyte permeability, such as through interfacial engineering by chemical reactions[198] or physical vapor deposition technology,[199] can isolate the electrolyte from the copper current collector and prevent the electrolyte from coming into contact with Li metal, thereby inhibiting Li cor-

rosion. Given that particular experimental techniques do not inherently align with the core tenets of electrolyte engineering, they are not elaborated upon in this discourse.

3.2.4   Others. In addition to improving SEI uniformity, and mechanical and chemical stability, there are some unconventional electrolyte engineering design concepts, such as the self-healing electrostatic shield (SHES) mechanism and the reactivation and reuse of dead Li, that can be employed to enhance the cycling CE of the Li anode. Ding *et al.* reported that introducing an appropriate concentration of cations (such as Cesium ions (Cs^+) or Rubidium ions (Rb^+)) as additives resulted in a reduction potential of Cs^+ in the electrolyte that was lower than that of Li^+. This enables Cs^+ to exist in the electrolyte in the form of cations and to be aggregated at the tip of the Li deposit, forming an electrostatic shield. This shield, formed through the repulsive effect between charges of the same kind, can effectively alleviate the "hotspot" effect in dendrite growth.[200]

In the cycling process of Li metal anodes, the formation and accumulation of dead Li are perpetual companions; this is a direct cause of battery capacity fading.[41] Jin *et al.* utilized triiodide anions (I_3^-) as a "dead Li activator", which could spontaneously react with Li metal fragments in "dead Li" and Li_2O in the SEI during battery cycling, converting dead Li into soluble Li iodide (LiI) and Li iodate ($LiIO_3$); LiI, acting as a "Li carrier", can migrate to the cathode side under the influence of a concentration gradient and be oxidized by the cathode material in the charging state, thereby recovering and storing Li ions.[201]

Overall, electrolyte engineering represents a pivotal strategy for enhancing the CE of the lithium anode under practical conditions. Optimization and regulation can facilitate improvements in cycling reversibility, cycle life and the safety of Li metal batteries. Nevertheless, this field of research still faces significant challenges. The selection of electrolyte components is primarily based on empirical trial and error, which is constrained by the lack of fundamental understanding of the mechanism of SEI formation on the Li surface and the influence of SEI characteristics on Li plating and stripping behaviors. It is therefore recommended that future research on electrolyte engineering should aim to gain a deeper understanding of the interaction between electrolyte and electrode materials, optimize interfacial compatibility and design more efficient electrolyte formulations in order to promote its popularity in practical applications.

4.   Conclusions and perspectives

The high CE of Li metal anodes is of pivotal significance for their practical applications. In particular, under practical conditions, the limitations of a restricted Li reservoir and lean electrolyte highlight the necessity for improving the CE of Li metal anodes. The primary determinants of CE encompass the generation of inactive Li^0 as a consequence of the formation of

Li dendrites and the irreversible capacity loss that is attributable to the continuous growth and reconstruction of the SEI. To date, researchers have endeavored to employ approaches, including composite Li anodes and electrolyte engineering strategies, to prepare Li metal anodes with an elevated CE under practical conditions, achieving CEs that surpass 99.0% and even approach 99.9%.

Nevertheless, as an anode material for Li batteries competing with graphite and silicon/graphite anodes, it is crucial to further enhance the cycle life of Li metal anodes under practical conditions to thousands of cycles. Therefore, the CE of Li metal anodes should move to 99.99%, presenting significant challenges for the future design of Li metal anodes. This endeavor must encompass, but is not limited to, the following considerations:

(1) *Unified and precise evaluation of CE for predicting the cycle life of Li metal batteries.* The CE in different publications is difficult to compare because CE is measured with various methods under different test conditions. It is imperative that CE is measured in accordance with a unfied method and test condition. The conventional method is suggested for its convenience. To meet the requirements of practical conditions with high energy density (>500 Wh kg^{-1}), a low N/P ratio is required, for which the areal capacity of the cathode is usually higher than 5.0 mAh cm^{-2}. Normal Li metal batteries are generally cycled at a current density of at least 1.0 mA cm^{-2}. Therefore, to make the test conditions as close as possible to the requirements of practical conditions, high cycle capacity and high current density conditions are necessary. 1.0 mA cm^{-2} and 5.0 mAh cm^{-2} are recommended as test conditions taking the battery practical conditions into consideration. It is important to acknowledge the significant difference in working conditions between coin and pouch cells. Due to limitations imposed by practical conditions, the N/P ratio and E/C ratio in pouch cells are considerably lower compared with those in coin cells. Concurrently, the uneven distribution of current density and electrolyte in the pouch cells, when compared with the coin cells, is not favorable for high CE. Consequently, the actual CE in pouch cells is typically lower than the CE measured in coin cells. Consequently, it is imperative to accurately measure the CE of Li metal anodes in pouch cells to better reflect the stability of Li metal anodes under practical conditions. The development of more precise and efficient evaluation methods is essential. When it comes to a high CE of >99.9%, the effect of the accuracy of the testing apparatus and the stability of the testing temperature on CE precision must be considered. Conventional test instruments for CE measurement exhibit an error of approximately 100 ppm.[202–204] For Li metal anodes with a CE of up to 99.9% or even 99.99%, this level of accuracy is inadequate. It is therefore essential to use an ultrahigh precision charger to enhance the measurement accuracy of CE, which requires precise control of the test temperature (±0.2 °C) and elevated standards for the precision of test parameters, including current and voltage.[203] Furthermore, although the conventional CE measurement approach is effective at assessing the stability of

Li metal anodes, there is not a clear relationship between the CE of Li metal anodes and the cycle life of Li metal batteries. A profound understanding of the correlation between the CE of Li metal anodes and the cycle life of Li metal batteries, as well as the establishment of quantitative relationships, are required.

(2) *Quantitative evaluation criteria for SEI properties.* The SEI plays a multifaceted role on the surface of Li metal anodes, facilitating the transport of Li ions, insulating electrons, and impeding the permeation of electrolyte components. The ion transport characteristics of the SEI notably influence the morphology of Li deposition, while its electronic insulation and capability to passivate the electrolyte dictate the propensity for side reactions between the electrolyte and the anode. Currently, to propel the CE beyond the threshold of 99.9%, it is imperative to minimize the capacity consumption associated with SEI growth and reconstruction. This necessitates a focused investigation into the intrinsic properties of the SEI, including but not limited to ion transport behavior, formation kinetics, and the passivation capability towards the electrolyte. Nevertheless, our understanding of the SEI remains somewhat vague, and there is a lack of systematic and quantitative evaluation metrics for the intrinsic characteristics of the SEI. Consequently, concerted efforts must be directed towards the establishment of criteria capable of providing a systematic and quantitative assessment of the intrinsic properties of the SEI, thereby rationally guiding the development of a more stable SEI to achieve Li metal anodes with higher CE. This endeavor requires the development of rigorous evaluation protocols, a detailed understanding of the SEI formation process, and the advancement of property characterization techniques. The model experiment is a promising approach for systematically evaluating SEI properties. By using inert substrates such as Cu and glassy carbon, an SEI with a similar composition and structure to those of the SEI of a Li metal anode can be obtained by electrochemical processes.[31,205] At the same time, chemical reactions on the surface of the blocking electrode can be decoupled from the ion transport process, and the properties of the SEI can be systematically quantified.[206,207] Furthermore, it is imperative to establish rational operational standards for the SEI formation process to ensure the comparability of the SEI across diverse electrolyte systems.

(3) *SEI with high uniformity, high mechanical stability, and high passivation capability.* As discussed in Section 2.5, the quest for an enhanced CE exceeding 99.9% is impeded by the irreversible capacity loss stemming from the relentless growth and reconstruction of the SEI, which is a direct consequence of inherent instability and the lack of compactness of the SEI. The current prevailing strategy to improve CE involves augmenting the inorganic fraction within the SEI to foster a uniform Li deposition morphology. However, it is crucial to recognize that an indiscriminate increase in inorganic content does not guarantee the desired stability and compactness of the SEI. For instance, when the inorganic particles within the SEI are of larger dimensions, the lack of compactness hinders the effective passivation of the electrolyte, thereby facilitating

the continuous growth of the SEI.[196] Moreover, inherent brittleness of inorganic materials can lead to SEI rupture under the substantial volumetric changes induced by Li plating/stripping, triggering the reconstruction of the SEI.[113] Consequently, beyond the imperative to suppress Li dendrite proliferation, there is a pressing need to engineer an SEI that embodies the ideal attributes of uniformity, mechanical stability, and effective passivation to electrolytes. To this end, judicious modulation of the organic-to-inorganic ratio within the SEI, and the refinement of charging/discharging protocols to diminish the size of inorganic particles, present viable avenues for the further optimization of SEI properties. These approaches not only promise to enhance the stability of the SEI to withstand the rigors of Li metal anodes during cycling but also to maintain a robust barrier against electrolyte degradation, thereby paving the way for high-CE Li metal anodes under practical conditions. Optimizing the composition and structure of the SEI requires the search for a broader range of electrolytes, including novel solvents, salts, and additives, especially using artificial intelligence for electrolyte design.

(4) *Advanced techniques for profiling the interactions in electrolytes.* The genesis of the SEI is intricately linked to inherent characteristics of the electrolyte. In this complex system, the interplay between solvent, anion, and Li ions is multifaceted, encompassing ionic bonds, Li bonds, and a spectrum of other interactions.[208–210] These complex forces exert a profound influence on the decomposition dynamics of electrolytes at the anode/electrolyte interface, thereby dictating the composition and structure of the SEI, further affecting the cycling performance of Li metal anodes. Consequently, there is a compelling need to develop advanced experimental characterization techniques to elucidate the microscopic interactions within the electrolyte. The ability to scrutinize these interaction forces is pivotal for deciphering the reaction kinetics of the electrolyte, which is essential for the rational design of the SEI. Nuclear magnetic resonance (NMR) technology emerges as a promising tool in this context, given its capacity to probe local environments within electrolytes.[211–213] Nevertheless, the clarification of minute interactions within the complex environment of electrolytes requires a more sophisticated experimental approach.

(5) *Reusing inactive Li.* Under practical conditions, the operation of Li metals inevitably results in the generation of inactive Li at the anode side. Even in the open-circuit state, Li metal anodes are susceptible to a calendar ageing process analogous to that observed in Li-ion batteries. This process results in the production of inactive Li and a concomitant reduction in capacity, which is likely to be more pronounced under practical conditions that necessitate a high charging capacity. It is therefore crucial to identify methods of reusing inactive Li during both the cycling and resting processes, with the aim of further improving the CE of the Li metal anode. Currently, several methods have been developed for the reuse of inactive Li, which have demonstrated efficacy for extending the cycle life of Li metal anodes.[214–216] However, further investment in the development of more effective methods for the reuse of

inactive Li on the anode side is necessary to further enhance the CE and cycle stability of Li metal anodes under practical conditions.

(6) *Machine learning and experimental insights for the design of high-CE Li metal anodes under practical conditions.* In the contemporary landscape of materials science, machine learning has emerged as a pivotal tool, facilitating the processes of data curation and theoretical abstraction.[217–223] Notwithstanding the discrepancies in experimental setups, a substantial corpus of empirical evidence has been accumulated, particularly with regard to the methodologies employed to enhance CE. The incorporation of machine learning methodologies to analyze these accumulated experimental outcomes is anticipated to facilitate the comprehension and formulation of critical factors or strategies aimed at enhancing the CE of Li metal anodes under practical conditions. In order to fully utilize the capabilities of machine learning, it is essential to have access to a substantial corpus of high-quality experimental data. It is therefore essential to meticulously document and provide the conditions for CE testing, the operational parameters of the battery, and the specifics of battery cycling, in order to ensure that the machine learning models are informed by a robust and detailed dataset. This approach is fundamental to the effective application of machine learning in the pursuit of higher CE Li metal anodes under practical conditions. Furthermore, the utilization of machine learning methodologies to assess a multitude of battery configurations and their respective cycle performance enables a comparison of the electrochemical properties of disparate systems. When coupled with digital twin technology, the battery performance data, electrochemical response signals, and material characteristics are synthesized, thereby establishing a digital model system that can predict the CE and electrochemical performance of diverse battery systems.

High CE is a fundamental requirement for the stable cycling of Li metal anodes under practical applications. The development of Li metal anodes has reached a significant milestone with the achievement of an impressive CE of 99.9%. Nevertheless, to meet the commercial aspirations for Li metal anodes capable of enduring thousands of cycles, it is imperative to pursue even higher levels of cycling stability, specifically a CE exceeding 99.99%. To achieve this ambitious target, it is essential that the battery community works collectively and rigorously to refine the design and regulation of Li metal battery systems through extensive research and innovation.

Data availability

No primary research results, software or code have been included and no new data were generated or analysed as part of this review.

Conflicts of interest

The authors have no conflict of interest.

Acknowledgements

References

1 S. Chu and A. Majumdar, *Nature*, 2012, **488**, 294–303.
2 D. Larcher and J. M. Tarascon, *Nat. Chem.*, 2015, **7**, 19–29.
3 J. Lu, T. Wu and K. Amine, *Nat. Energy*, 2017, **2**, 17011.
4 J.-L. Li, L. Shen, Z.-N. Cheng, J.-D. Zhang, L.-X. Li, Y.-T. Zhang, Y.-B. Gao, C. Guo, X. Chen, C.-Z. Zhao, R. Zhang and Q. Zhang, *J. Energy Chem.*, 2025, **101**, 16–22.
5 M. S. Whittingham, *Chem. Rev.*, 2004, **104**, 4271–4302.
6 B. Scrosati and J. Garche, *J. Power Sources*, 2010, **195**, 2419–2430.
7 S. Chu, Y. Cui and N. Liu, *Nat. Mater.*, 2017, **16**, 16–22.
8 X.-Y. Li, S. Feng, C.-X. Zhao, Q. Cheng, Z.-X. Chen, S.-Y. Sun, X. Chen, X.-Q. Zhang, B.-Q. Li, J.-Q. Huang and Q. Zhang, *J. Am. Chem. Soc.*, 2022, **144**, 14638–14646.
9 B. Cao, M. Du, Z. Guo, H. Liu, C. Yan, A. Chen, X. Chen, C. Tang, J.-Q. Huang and Q. Zhang, *Carbon Future*, 2024, **1**, 9200017.
10 W.-Z. Huang, P. Xu, X.-Y. Huang, C.-Z. Zhao, X. Bie, H. Zhang, A. Chen, E. Kuzmina, E. Karaseva, V. Kolosnitsyn, X. Zhai, T. Jiang, L.-Z. Fan, D. Wang and Q. Zhang, *MetalMat*, 2024, **1**, e6.
11 Y. Yang, L. Xu, C. Yan, J.-Q. Huang and Q. Zhang, *Energy Lab*, 2023, **1**, 220011.
12 Q. Man, Y. An, C. Liu, H. Shen, S. Xiong and J. Feng, *J. Energy Chem.*, 2023, **76**, 576–600.
13 R. Marom, S. F. Amalraj, N. Leifer, D. Jacob and D. Aurbach, *J. Mater. Chem.*, 2011, **21**, 9938–9954.
14 M. V. Reddy, A. Mauger, C. M. Julien, A. Paolella and K. Zaghib, *Materials*, 2020, **13**, 1884.
15 N. Nitta, F. Wu, J. T. Lee and G. Yushin, *Mater. Today*, 2015, **18**, 252–264.
16 J. M. Tarascon and M. Armand, *Nature*, 2001, **414**, 359–367.
17 J.-F. Ding, Y.-T. Zhang, R. Xu, R. Zhang, Y. Xiao, S. Zhang, C.-X. Bi, C. Tang, R. Xiang, H. S. Park, Q. Zhang and J.-Q. Huang, *Green Energy Environ.*, 2023, **8**, 1509–1530.
18 Q. Cheng, Z.-X. Chen, X.-Y. Li, L.-P. Hou, C.-X. Bi, X.-Q. Zhang, J.-Q. Huang and B.-Q. Li, *J. Energy Chem.*, 2023, **76**, 181–186.
19 H. Adenusi, G. A. Chass, S. Passerini, K. V. Tian and G. Chen, *Adv. Energy Mater.*, 2023, **13**, 2203307.

20 X.-B. Cheng, R. Zhang, C.-Z. Zhao and Q. Zhang, *Chem. Rev.*, 2017, **117**, 10403–10473.

21 U. S. Meda, L. Lal, S. M and P. Garg, *J. Energy Storage*, 2022, **47**, 103564.

22 X. Zhang, X. Cheng and Q. Zhang, *J. Energy Chem.*, 2016, **25**, 967–984.

23 A. Kushima, K. P. So, C. Su, P. Bai, N. Kuriyama, T. Maebashi, Y. Fujiwara, M. Z. Bazant and J. Li, *Nano Energy*, 2017, **32**, 271–279.

24 Z. Tong, B. Bazri, S.-F. Hu and R.-S. Liu, *J. Mater. Chem. A*, 2021, **9**, 7396–7406.

25 M.-Y. Zhou, X.-Q. Ding, J.-F. Ding, L.-P. Hou, P. Shi, J. Xie, B.-Q. Li, J.-Q. Huang, X.-Q. Zhang and Q. Zhang, *Joule*, 2022, **6**, 2122–2137.

26 C.-X. Bi, L.-P. Hou, Z. Li, M. Zhao, X.-Q. Zhang, B.-Q. Li, Q. Zhang and J.-Q. Huang, *Energy Mater. Adv.*, 2023, **4**, 0010.

27 J. Xiao, Q. Li, Y. Bi, M. Cai, B. Dunn, T. Glossmann, J. Liu, T. Osaka, R. Sugiura, B. Wu, J. Yang, J.-G. Zhang and M. S. Whittingham, *Nat. Energy*, 2020, **5**, 561–568.

28 J. Liu, Z. Bao, Y. Cui, E. J. Dufek, J. B. Goodenough, P. Khalifah, Q. Li, B. Y. Liaw, P. Liu, A. Manthiram, Y. S. Meng, V. R. Subramanian, M. F. Toney, V. V. Viswanathan, M. S. Whittingham, J. Xiao, W. Xu, J. Yang, X.-Q. Yang and J.-G. Zhang, *Nat. Energy*, 2019, **4**, 180–186.

29 X.-Y. Li, S. Feng, Y.-W. Song, C.-X. Zhao, Z. Li, Z.-X. Chen, Q. Cheng, X. Chen, X.-Q. Zhang, B.-Q. Li, J.-Q. Huang and Q. Zhang, *J. Am. Chem. Soc.*, 2024, **146**, 14754–14764.

30 A. Mohammadi, S. Djafer, S. Sayegh, A. J. Naylor, M. Bechelany, R. Younesi, L. Monconduit and L. Stievano, *Chem. Mater.*, 2023, **35**, 2381–2393.

31 S.-Y. Sun, N. Yao, C.-B. Jin, J. Xie, X.-Y. Li, M.-Y. Zhou, X. Chen, B.-Q. Li, X.-Q. Zhang and Q. Zhang, *Angew. Chem., Int. Ed.*, 2022, **61**, e202208743.

32 D. Lin, Y. Liu and Y. Cui, *Nat. Nanotechnol.*, 2017, **12**, 194–206.

33 X. Shan, Y. Zhong, L. Zhang, Y. Zhang, X. Xia, X. Wang and J. Tu, *J. Phys. Chem. C*, 2021, **125**, 19060–19080.

34 H. Wang, Z. Yu, X. Kong, S. C. Kim, D. T. Boyle, J. Qin, Z. Bao and Y. Cui, *Joule*, 2022, **6**, 588–616.

35 X. Zhang, Y. Yang and Z. Zhou, *Chem. Soc. Rev.*, 2020, **49**, 3040–3071.

36 C. Wei, Y. Zhang, Y. Tian, L. Tan, Y. An, Y. Qian, B. Xi, S. Xiong, J. Feng and Y. Qian, *Energy Storage Mater.*, 2021, **38**, 157–189.

37 L.-P. Hou, X.-Q. Zhang, B.-Q. Li and Q. Zhang, *Mater. Today*, 2021, **45**, 62–76.

38 X. He, D. Bresser, S. Passerini, F. Baakes, U. Krewer, J. Lopez, C. T. Mallia, Y. Shao-Horn, I. Cekic-Laskovic, S. Wiemers-Meyer, F. A. Soto, V. Ponce, J. M. Seminario, P. B. Balbuena, H. Jia, W. Xu, Y. Xu, C. Wang, B. Horstmann, R. Amine, C.-C. Su, J. Shi, K. Amine, M. Winter, A. Latz and R. Kostecki, *Nat. Rev. Mater.*, 2021, **6**, 1036–1052.

39 J.-F. Ding, R. Xu, Y. Xiao, S. Zhang, T.-L. Song, C. Yan and J.-Q. Huang, *Adv. Energy Mater.*, 2023, **13**, 2204305.

40 N. Yao, S.-Y. Sun, X. Chen, X.-Q. Zhang, X. Shen, Z.-H. Fu, R. Zhang and Q. Zhang, *Angew. Chem., Int. Ed.*, 2022, **61**, e202210859.

41 C. Fang, J. Li, M. Zhang, Y. Zhang, F. Yang, J. Z. Lee, M.-H. Lee, J. Alvarado, M. A. Schroeder, Y. Yang, B. Lu, N. Williams, M. Ceja, L. Yang, M. Cai, J. Gu, K. Xu, X. Wang and Y. S. Meng, *Nature*, 2019, **572**, 511–515.

42 I. Yoshimatsu, T. Hirai and J. Yamaki, *J. Electrochem. Soc.*, 1988, **135**, 2422–2427.

43 D. Lu, Y. Shao, T. Lozano, W. D. Bennett, G. L. Graff, B. Polzin, J. Zhang, M. H. Engelhard, N. T. Saenz, W. A. Henderson, P. Bhattacharya, J. Liu and J. Xiao, *Adv. Energy Mater.*, 2015, **5**, 1400993.

44 Y.-X. Yao, C. Yan and Q. Zhang, *Chem. Commun.*, 2020, **56**, 14570–14584.

45 S. Zhang, M. S. Ding, K. Xu, J. Allen and T. R. Jow, *Electrochem. Solid-State Lett.*, 2001, **4**, A206–A208.

46 S.-Y. Sun, X.-Q. Zhang, Y.-N. Wang, J.-L. Li, Z. Zheng and J.-Q. Huang, *Mater. Today*, 2024, **77**, 39–65.

47 Z. Li, L. Wang, X. Huang and X. He, *Small*, 2024, **20**, 2305429.

48 Z. Zhang, Y. Li, R. Xu, W. Zhou, Y. Li, S. T. Oyakhire, Y. Wu, J. Xu, H. Wang, Z. Yu, D. T. Boyle, W. Huang, Y. Ye, H. Chen, J. Wan, Z. Bao, W. Chiu and Y. Cui, *Science*, 2022, **375**, 66–70.

49 P. Sayavong, W. Zhang, S. T. Oyakhire, D. T. Boyle, Y. Chen, S. C. Kim, R. A. Vilá, S. E. Holmes, M. S. Kim, S. F. Bent, Z. Bao and Y. Cui, *J. Am. Chem. Soc.*, 2023, **145**, 12342–12350.

50 S. Yuan, T. Kong, Y. Zhang, P. Dong, Y. Zhang, X. Dong, Y. Wang and Y. Xia, *Angew. Chem., Int. Ed.*, 2021, **60**, 25624–25638.

51 S. Kim, G. Park, S. J. Lee, S. Seo, K. Ryu, C. H. Kim and J. W. Choi, *Adv. Mater.*, 2023, **35**, 2206625.

52 Z. Li, Y.-X. Yao, S. Sun, C.-B. Jin, N. Yao, C. Yan and Q. Zhang, *Angew. Chem., Int. Ed.*, 2023, **62**, e202303888.

53 P. Shi, X.-Q. Zhang, X. Shen, R. Zhang, H. Liu and Q. Zhang, *Adv. Mater. Technol.*, 2020, **5**, 1900806.

54 T. Li, H. Liu, P. Shi and Q. Zhang, *Rare Met.*, 2018, **37**, 449–458.

55 X.-B. Cheng, C.-Z. Zhao, Y.-X. Yao, H. Liu and Q. Zhang, *Chem*, 2019, **5**, 74–96.

56 Y. Yamada, Y. Iriyama, T. Abe and Z. Ogumi, *Langmuir*, 2009, **25**, 12766–12770.

57 J.-G. Zhang, W. Xu, J. Xiao, X. Cao and J. Liu, *Chem. Rev.*, 2020, **120**, 13312–13348.

58 S. Li, M. Jiang, Y. Xie, H. Xu, J. Jia and J. Li, *Adv. Mater.*, 2018, **30**, 1706375.

59 Y. Zhu, V. Pande, L. Li, B. Wen, M. S. Pan, D. Wang, Z.-F. Ma, V. Viswanathan and Y.-M. Chiang, *Proc. Natl. Acad. Sci. U. S. A.*, 2020, **117**, 27195–27203.

60 Z. Luo, Y. Cao, G. Xu, W. Sun, X. Xiao, H. Liu and S. Wang, *Carbon Neutralization*, 2024, **3**, 647–672.

61 R. Schmuch, R. Wagner, G. Hörpel, T. Placke and M. Winter, *Nat. Energy*, 2018, **3**, 267–278.

62 M. Winter, B. Barnett and K. Xu, *Chem. Rev.*, 2018, **118**, 11433–11456.

63 K. Xu, *Nat. Energy*, 2021, **6**, 763–763.

64 Z. Wei, Z. Shi, X. Wen, X. Li, B. Qiu, Q. Gu, J. Sun, Y. Han, H. Luo, H. Guo, Y. Xia, C. Yin, P. Cai and Z. Liu, *Mater. Today Energy*, 2022, **27**, 101039.

65 X. Ou, T. Liu, W. Zhong, X. Fan, X. Guo, X. Huang, L. Cao, J. Hu, B. Zhang, Y. S. Chu, G. Hu, Z. Lin, M. Dahbi, J. Alami, K. Amine, C. Yang and J. Lu, *Nat. Commun.*, 2022, **13**, 2319.

66 Y. Jie, C. Tang, Y. Xu, Y. Guo, W. Li, Y. Chen, H. Jia, J. Zhang, M. Yang, R. Cao, Y. Lu, J. Cho and S. Jiao, *Angew. Chem., Int. Ed.*, 2024, **63**, e202307802.

67 C. Niu, H. Lee, S. Chen, Q. Li, J. Du, W. Xu, J.-G. Zhang, M. S. Whittingham, J. Xiao and J. Liu, *Nat. Energy*, 2019, **4**, 551–559.

68 C. Niu, D. Liu, J. A. Lochala, C. S. Anderson, X. Cao, M. E. Gross, W. Xu, J.-G. Zhang, M. S. Whittingham, J. Xiao and J. Liu, *Nat. Energy*, 2021, **6**, 723–732.

69 G. S. Mattei, Z. Li, A. A. Corrao, C. Niu, Y. Zhang, B. Liaw, C. C. Dickerson, J. Xiao, E. J. Dufek and P. G. Khalifah, *Chem. Mater.*, 2021, **33**, 2378–2386.

70 B. Horstmann, J. Shi, R. Amine, M. Werres, X. He, H. Jia, F. Hausen, I. Cekic-Laskovic, S. Wiemers-Meyer, J. Lopez, D. Galvez-Aranda, F. Baakes, D. Bresser, C.-C. Su, Y. Xu, W. Xu, P. Jakes, R.-A. Eichel, E. Figgemeier, U. Krewer, J. M. Seminario, P. B. Balbuena, C. Wang, S. Passerini, Y. Shao-Horn, M. Winter, K. Amine, R. Kostecki and A. Latz, *Energy Environ. Sci.*, 2021, **14**, 5289–5314.

71 C.-J. Huang, B. Thirumalraj, H.-C. Tao, K. N. Shitaw, H. Sutiono, T. T. Hagos, T. T. Beyene, L.-M. Kuo, C.-C. Wang, S.-H. Wu, W.-N. Su and B. J. Hwang, *Nat. Commun.*, 2021, **12**, 1452.

72 S. Chen, C. Niu, H. Lee, Q. Li, L. Yu, W. Xu, J.-G. Zhang, E. J. Dufek, M. S. Whittingham, S. Meng, J. Xiao and J. Liu, *Joule*, 2019, **3**, 1094–1105.

73 J. Xiao, *Science*, 2019, **366**, 426–427.

74 S. C. Nagpure, T. R. Tanim, E. J. Dufek, V. V. Viswanathan, A. J. Crawford, S. M. Wood, J. Xiao, C. C. Dickerson and B. Liaw, *J. Power Sources*, 2018, **407**, 53–62.

75 B. D. Adams, J. Zheng, X. Ren, W. Xu and J.-G. Zhang, *Adv. Energy Mater.*, 2018, **8**, 1702097.

76 J. Zheng, P. Yan, D. Mei, M. H. Engelhard, S. S. Cartmell, B. J. Polzin, C. Wang, J.-G. Zhang and W. Xu, *Adv. Energy Mater.*, 2016, **6**, 1502151.

77 P. Albertus, S. Babinec, S. Litzelman and A. Newman, *Nat. Energy*, 2018, **3**, 16–21.

78 J. Zheng, T. Tang, Q. Zhao, X. Liu, Y. Deng and L. A. Archer, *ACS Energy Lett.*, 2019, **4**, 1349–1355.

79 E. Winter, T. J. Schmidt and S. Trabesinger, *Batteries Supercaps*, 2022, **5**, e202100145.

80 D. Aurbach, O. Youngman, Y. Gofer and A. Meitav, *Electrochim. Acta*, 1990, **35**, 625–638.

81 D. Aurbach and E. Granot, *Electrochim. Acta*, 1997, **42**, 697–718.

82 F. Ding, W. Xu, X. Chen, J. Zhang, M. H. Engelhard, Y. Zhang, B. R. Johnson, J. V. Crum, T. A. Blake, X. Liu and J.-G. Zhang, *J. Electrochem. Soc.*, 2013, **160**, A1894–A1901.

83 S. V. Sazhin, A. V. Gorodyskii, M. Y. Khimchenko, S. P. Kuksenko and V. V. Danilin, *J. Electroanal. Chem.*, 1993, **344**, 61–72.

84 J. Qian, B. D. Adams, J. Zheng, W. Xu, W. A. Henderson, J. Wang, M. E. Bowden, S. Xu, J. Hu and J.-G. Zhang, *Adv. Funct. Mater.*, 2016, **26**, 7094–7102.

85 J. Z. Lee, T. A. Wynn, M. A. Schroeder, J. Alvarado, X. Wang, K. Xu and Y. S. Meng, *ACS Energy Lett.*, 2019, **4**, 489–493.

86 G. M. Hobold, J. Lopez, R. Guo, N. Minafra, A. Banerjee, Y. S. Meng, Y. Shao-Horn and B. M. Gallant, *Nat. Energy*, 2021, **6**, 951–960.

87 R. Selim and P. Bro, *J. Electrochem. Soc.*, 1974, **121**, 1457–1459.

88 R. D. Rauh and S. B. Brummer, *Electrochim. Acta*, 1977, **22**, 75–83.

89 Y.-C. Hsieh, M. Leißing, S. Nowak, B.-J. Hwang, M. Winter and G. Brunklaus, *Cell Rep. Phys. Sci.*, 2020, **1**, 100139.

90 A. B. Gunnarsdóttir, C. V. Amanchukwu, S. Menkin and C. P. Grey, *J. Am. Chem. Soc.*, 2020, **142**, 20814–20827.

91 D. T. Boyle, W. Huang, H. Wang, Y. Li, H. Chen, Z. Yu, W. Zhang, Z. Bao and Y. Cui, *Nat. Energy*, 2021, **6**, 487–494.

92 X. He, K. Zhang, Z. Zhu, Z. Tong and X. Liang, *Chem. Soc. Rev.*, 2024, **53**, 9–24.

93 S. Park, H.-J. Jin and Y. S. Yun, *Adv. Mater.*, 2020, **32**, 2002193.

94 H. Wu, H. Jia, C. Wang, J.-G. Zhang and W. Xu, *Adv. Energy Mater.*, 2021, **11**, 2003092.

95 Q. Zhao, S. Stalin and L. A. Archer, *Joule*, 2021, **5**, 1119–1142.

96 K. Kim, H. Ma, S. Park and N.-S. Choi, *ACS Energy Lett.*, 2020, **5**, 1537–1553.

97 Y. S. Meng, V. Srinivasan and K. Xu, *Science*, 2022, **378**, eabq3750.

98 L. Liu, Y.-X. Yin, J.-Y. Li, N.-W. Li, X.-X. Zeng, H. Ye, Y.-G. Guo and L.-J. Wan, *Joule*, 2017, **1**, 563–575.

99 K. Lin, X. Xu, X. Qin, G. Zhang, M. Liu, F. Lv, Y. Xia, F. Kang, G. Chen and B. Li, *Energy Storage Mater.*, 2020, **26**, 250–259.

100 L. Luo, J. Li, H. Yaghoobnejad Asl and A. Manthiram, *Adv. Mater.*, 2019, **31**, 1904537.

101 G. Li, Z. Liu, Q. Huang, Y. Gao, M. Regula, D. Wang, L.-Q. Chen and D. Wang, *Nat. Energy*, 2018, **3**, 1076–1083.

102 H. Gan, R. Wang, J. Wu, H. Chen, R. Li and H. Liu, *ACS Appl. Mater. Interfaces*, 2021, **13**, 37162–37171.

103 H. Zhang, X. Liao, Y. Guan, Y. Xiang, M. Li, W. Zhang, X. Zhu, H. Ming, L. Lu, J. Qiu, Y. Huang, G. Cao, Y. Yang, L. Mai, Y. Zhao and H. Zhang, *Nat. Commun.*, 2018, **9**, 3729.

104 J. Xiang, L. Yuan, Y. Shen, Z. Cheng, K. Yuan, Z. Guo, Y. Zhang, X. Chen and Y. Huang, *Adv. Energy Mater.*, 2018, **8**, 1802352.

105 P. Qing, Z. Wu, A. Wang, S. Huang, K. Long, T. Naren, D. Chen, P. He, H. Huang, Y. Chen, L. Mei and L. Chen, *Adv. Mater.*, 2023, **35**, 2211203.

106 S. Chen, J. Zheng, D. Mei, K. S. Han, M. H. Engelhard, W. Zhao, W. Xu, J. Liu and J.-G. Zhang, *Adv. Mater.*, 2018, **30**, 1706102.

107 C. Yan, H.-R. Li, X. Chen, X.-Q. Zhang, X.-B. Cheng, R. Xu, J.-Q. Huang and Q. Zhang, *J. Am. Chem. Soc.*, 2019, **141**, 9422–9429.

108 Y. Yang, Y. Yin, D. M. Davies, M. Zhang, M. Mayer, Y. Zhang, E. S. Sablina, S. Wang, J. Z. Lee, O. Borodin, C. S. Rustomji and Y. S. Meng, *Energy Environ. Sci.*, 2020, **13**, 2209–2219.

109 R. Xu, J.-F. Ding, X.-X. Ma, C. Yan, Y.-X. Yao and J.-Q. Huang, *Adv. Mater.*, 2021, **33**, 2105962.

110 Z. Yu, P. E. Rudnicki, Z. Zhang, Z. Huang, H. Celik, S. T. Oyakhire, Y. Chen, X. Kong, S. C. Kim, X. Xiao, H. Wang, Y. Zheng, G. A. Kamat, M. S. Kim, S. F. Bent, J. Qin, Y. Cui and Z. Bao, *Nat. Energy*, 2022, **7**, 94–106.

111 G. Zhang, J. Li, Q. Wang, H. Wang, J. Wang, K. Yu, J. Chang, C. Wang, X. Hong, Q. Ma and Y. Deng, *ACS Energy Lett.*, 2023, **8**, 2868–2877.

112 S. Zhang, R. Li, T. Deng, Q. Ma, X. Hong, H. Zhang, R. Zhang, S. Ding, Y. Wu, H. Zhu, M. Li, H. Zhang, D. Lu, B. Ma, L. Lv, Y. Li, L. Chen, Y. Shen, R. Guo and X. Fan, *Nat. Energy*, 2024, **9**, 1285–1296.

113 Q.-K. Zhang, X.-Q. Zhang, J. Wan, N. Yao, T.-L. Song, J. Xie, L.-P. Hou, M.-Y. Zhou, X. Chen, B.-Q. Li, R. Wen, H.-J. Peng, Q. Zhang and J.-Q. Huang, *Nat. Energy*, 2023, **8**, 725–735.

114 J.-A. Lee, S. Kim, Y. Cho, S. H. Kweon, H. Kang, J. H. Byun, E. Kwon, S. Seo, W. Kim, K. H. Ryu, S. K. Kwak, S. Hong and N.-S. Choi, *Adv. Sci.*, 2024, **11**, 2310094.

115 K. Yan, H.-W. Lee, T. Gao, G. Zheng, H. Yao, H. Wang, Z. Lu, Y. Zhou, Z. Liang, Z. Liu, S. Chu and Y. Cui, *Nano Lett.*, 2014, **14**, 6016–6022.

116 J. Chen, J. Zhao, L. Lei, P. Li, J. Chen, Y. Zhang, Y. Wang, Y. Ma and D. Wang, *Nano Lett.*, 2020, **20**, 3403–3410.

117 L. Chen, X. Fan, X. Ji, J. Chen, S. Hou and C. Wang, *Joule*, 2019, **3**, 732–744.

118 Z. Tu, P. Nath, Y. Lu, M. D. Tikekar and L. A. Archer, *Acc. Chem. Res.*, 2015, **48**, 2947–2956.

119 J. N. Chazalviel, *Phys. Rev. A*, 1990, **42**, 7355–7367.

120 Q. Xu, Y. Yang and H. Shao, *Phys. Chem. Chem. Phys.*, 2015, **17**, 20398–20406.

121 D. R. Ely and R. E. García, *J. Electrochem. Soc.*, 2013, **160**, A662–A668.

122 A. Pei, G. Zheng, F. Shi, Y. Li and Y. Cui, *Nano Lett.*, 2017, **17**, 1132–1139.

123 Y. Yang, J. Xiong, J. Zeng, J. Huang and J. Zhao, *Chem. Commun.*, 2018, **54**, 1178–1181.

124 R. Zhang, X.-B. Cheng, C.-Z. Zhao, H.-J. Peng, J.-L. Shi, J.-Q. Huang, J. Wang, F. Wei and Q. Zhang, *Adv. Mater.*, 2016, **28**, 2155–2162.

125 Z. Sun, S. Jin, H. Jin, Z. Du, Y. Zhu, A. Cao, H. Ji and L.-J. Wan, *Adv. Mater.*, 2018, **30**, 1800884.

126 Y. Chen, A. Elangovan, D. Zeng, Y. Zhang, H. Ke, J. Li, Y. Sun and H. Cheng, *Adv. Funct. Mater.*, 2020, **30**, 1906444.

127 J. Xiang, Y. Zhao, L. Yuan, C. Chen, Y. Shen, F. Hu, Z. Hao, J. Liu, B. Xu and Y. Huang, *Nano Energy*, 2017, **42**, 262–268.

128 S. Jin, Z. Sun, Y. Guo, Z. Qi, C. Guo, X. Kong, Y. Zhu and H. Ji, *Adv. Mater.*, 2017, **29**, 1700783.

129 D. Cao, Y. Jiao, Q. Cai, D. Han, Q. Zhang, Y. Ma, A. Dong and H. Zhu, *J. Mater. Chem. A*, 2019, **7**, 3289–3297.

130 Q. Meng, B. Deng, H. Zhang, B. Wang, W. Zhang, Y. Wen, H. Ming, X. Zhu, Y. Guan, Y. Xiang, M. Li, G. Cao, Y. Yang, H. Peng, H. Zhang and Y. Huang, *Energy Storage Mater.*, 2019, **16**, 419–425.

131 N. Zhu, Y. Yang, Y. Li, Y. Bai, J. Rong and C. Wu, *Carbon Energy*, 2024, **6**, e423.

132 L. Chen, H. Liu, M. Li, S. Zhou, F. Mo, S. Yu and J. Wei, *Batteries*, 2023, **9**, 391.

133 X. Yan, L. Lin, Q. Chen, Q. Xie, B. Qu, L. Wang and D.-L. Peng, *Carbon Energy*, 2021, **3**, 303–329.

134 S.-S. Chi, Y. Liu, W.-L. Song, L.-Z. Fan and Q. Zhang, *Adv. Funct. Mater.*, 2017, **27**, 1700348.

135 S.-H. Wang, Y.-X. Yin, T.-T. Zuo, W. Dong, J.-Y. Li, J.-L. Shi, C.-H. Zhang, N.-W. Li, C.-J. Li and Y.-G. Guo, *Adv. Mater.*, 2017, **29**, 1703729.

136 C.-P. Yang, Y.-X. Yin, S.-F. Zhang, N.-W. Li and Y.-G. Guo, *Nat. Commun.*, 2015, **6**, 8058.

137 Y. Sun, W. Zhao, X. Wang, M. Gao, X. Yang, K. Zhang, H. Zhao, Y. Bai and C. Wu, *Appl. Surf. Sci.*, 2022, **598**, 153785.

138 J. Cao, G. Qian, X. Lu and X. Lu, *Small*, 2023, **19**, 2205653.

139 K. Yan, Z. Lu, H.-W. Lee, F. Xiong, P.-C. Hsu, Y. Li, J. Zhao, S. Chu and Y. Cui, *Nat. Energy*, 2016, **1**, 16010.

140 E. Cha, J. H. Yun, R. Ponraj and D. K. Kim, *Mater. Chem. Front.*, 2021, **5**, 6294–6314.

141 Y. Wang, J. Tan, Z. Li, L. Ma, Z. Liu, M. Ye and J. Shen, *Energy Storage Mater.*, 2022, **53**, 156–182.

142 Y. Li, Y. Li, L. Zhang, H. Tao, Q. Li, J. Zhang and X. Yang, *J. Energy Chem.*, 2023, **77**, 123–136.

143 T. Liu, X. Chen, C. Zhan, X. Cao, Y. Wang and J.-H. Liu, *ChemNanoMat*, 2020, **6**, 1200–1207.

144 S. Cui, P. Zhai, W. Yang, Y. Wei, J. Xiao, L. Deng and Y. Gong, *Small*, 2020, **16**, 1905620.

145 Z. Yang, Q. Ruan, Y. Xiong and X. Gu, *Batteries*, 2023, **9**, 30.

146 R. Zhang, X.-R. Chen, X. Chen, X.-B. Cheng, X.-Q. Zhang, C. Yan and Q. Zhang, *Angew. Chem., Int. Ed.*, 2017, **56**, 7764–7768.

147 T. Wang, P. Zhai, D. Legut, L. Wang, X. Liu, B. Li, C. Dong, Y. Fan, Y. Gong and Q. Zhang, *Adv. Energy Mater.*, 2019, **9**, 1804000.

148 Y. Zhou, K. Zhao, Y. Han, Z. Sun, H. Zhang, L. Xu, Y. Ma and Y. Chen, *J. Mater. Chem. A*, 2019, **7**, 5712–5718.

149 Y. Zhu, Y. Yang, H. Zhang, S. Liu, Z. Wu, C. Wu, X. Gao, E. Hu and Z. Chen, *J. Colloid Interface Sci.*, 2023, **648**, 299–307.

150 K. Lin, X. Qin, M. Liu, X. Xu, G. Liang, J. Wu, F. Kang, G. Chen and B. Li, *Adv. Funct. Mater.*, 2019, **29**, 1903229.

151 Z. Li, Q. He, C. Zhou, Y. Li, Z. Liu, X. Hong, X. Xu, Y. Zhao and L. Mai, *Energy Storage Mater.*, 2021, **37**, 40–46.

152 Y.-X. Zhan, P. Shi, X.-X. Ma, C.-B. Jin, Q.-K. Zhang, S.-J. Yang, B.-Q. Li, X.-Q. Zhang and J.-Q. Huang, *Adv. Energy Mater.*, 2022, **12**, 2103291.

153 P. Bai, J. Li, F. R. Brushett and M. Z. Bazant, *Energy Environ. Sci.*, 2016, **9**, 3221–3229.

154 W. Cao, Q. Li, X. Yu and H. Li, *eScience*, 2022, **2**, 47–78.

155 S. Yuan, S. Weng, F. Wang, X. Dong, Y. Wang, Z. Wang, C. Shen, J. L. Bao, X. Wang and Y. Xia, *Nano Energy*, 2021, **83**, 105847.

156 Q. Zhao, Z. Tu, S. Wei, K. Zhang, S. Choudhury, X. Liu and L. A. Archer, *Angew. Chem., Int. Ed.*, 2018, **57**, 992–996.

157 F. Shen, F. Zhang, Y. Yin, S. Chen, J. Gao, J. Li and X. Han, *Nanoscale*, 2021, **13**, 11800–11807.

158 D. Tang, L. Yuan, Y. Liao, W. Jin, J. Chen, Z. Cheng, X. Li, B. He, Z. Li and Y. Huang, *Sci. China Mater.*, 2022, **65**, 2385–2392.

159 W. Zhang, H. L. Zhuang, L. Fan, L. Gao and Y. Lu, *Sci. Adv.*, 2018, **4**, eaar4410.

160 Z. Liang, G. Zheng, C. Liu, N. Liu, W. Li, K. Yan, H. Yao, P.-C. Hsu, S. Chu and Y. Cui, *Nano Lett.*, 2015, **15**, 2910–2916.

161 L. Fan, H. L. Zhuang, W. Zhang, Y. Fu, Z. Liao and Y. Lu, *Adv. Energy Mater.*, 2018, **8**, 1703360.

162 P. Shi, Z.-Y. Liu, X.-Q. Zhang, X. Chen, N. Yao, J. Xie, C.-B. Jin, Y.-X. Zhan, G. Ye, J.-Q. Huang, S. Ifan E L, T. Maria-Magdalena and Q. Zhang, *J. Energy Chem.*, 2022, **64**, 172–178.

163 C. Gao, J. Kang, Y. Zhang, C. He, C. Shi, B. Chen, L. Ma, E. Liu, J. Sha, F. Zhou and N. Zhao, *Chem. Commun.*, 2024, **60**, 9130–9148.

164 Y. Nan, S. Li, Y. Shi, S. Yang and B. Li, *Small*, 2019, **15**, 1903520.

165 J. Pu, J. Li, K. Zhang, T. Zhang, C. Li, H. Ma, J. Zhu, P. V. Braun, J. Lu and H. Zhang, *Nat. Commun.*, 2019, **10**, 1896.

166 H.-J. Noh, M.-H. Lee, B. G. Kim, J.-H. Park, S.-M. Lee and J.-H. Choi, *ACS Appl. Mater. Interfaces*, 2021, **13**, 55227–55234.

167 E. Peled, *J. Electrochem. Soc.*, 1979, **126**, 2047–2051.

168 Z. Li, Y.-X. Yao, M. Zheng, S. Sun, Y. Yang, Y. Xiao, L. Xu, C.-B. Jin, X.-Y. Yue, T. Song, P. Wu, C. Yan and Q. Zhang, *Angew. Chem., Int. Ed.*, 2025, **64**, e202409409.

169 S.-J. Yang, F.-N. Jiang, J.-K. Hu, H. Yuan, X.-B. Cheng, S. Kaskel, Q. Zhang and J.-Q. Huang, *Electron*, 2023, **1**, e8.

170 B. Jagger and M. Pasta, *Joule*, 2023, **7**, 2228–2244.

171 J.-L. Liang, S.-Y. Sun, N. Yao, Z. Zheng, Q.-K. Zhang, B.-Q. Li, X.-Q. Zhang and J.-Q. Huang, *Sci. China: Chem.*, 2023, **66**, 3620–3627.

172 X. Cao, H. Jia, W. Xu and J.-G. Zhang, *J. Electrochem. Soc.*, 2021, **168**, 010522.

173 T. Li, Z. Chen, F. Bai, C. Li and Y. Li, *J. Energy Chem.*, 2023, **81**, 404–409.

174 C. Wang, T. Ouyang, X. Wang, S. Liu, G. Tian, F. Fan, P. Liu, S. Wang, C. Zeng and C. Shu, *J. Energy Chem.*, 2024, **99**, 384–392.

175 Z. Deng, Y. Jia, Y. Deng, C. Xu, X. Zhang, Q. He, J. Peng, H. Wu and W. Cai, *J. Energy Chem.*, 2024, **96**, 282–290.

176 R. Xu, C. Yan, Y. Xiao, M. Zhao, H. Yuan and J.-Q. Huang, *Energy Storage Mater.*, 2020, **28**, 401–406.

177 L. Suo, W. Xue, M. Gobet, S. G. Greenbaum, C. Wang, Y. Chen, W. Yang, Y. Li and J. Li, *Proc. Natl. Acad. Sci. U. S. A.*, 2018, **115**, 1156–1161.

178 Y. Yamada, K. Furukawa, K. Sodeyama, K. Kikuchi, M. Yaegashi, Y. Tateyama and A. Yamada, *J. Am. Chem. Soc.*, 2014, **136**, 5039–5046.

179 J. Zhang, H. Zhang, R. Li, L. Lv, D. Lu, S. Zhang, X. Xiao, S. Geng, F. Wang, T. Deng, L. Chen and X. Fan, *J. Energy Chem.*, 2023, **78**, 71–79.

180 R. Wang, J. Li, B. Han, Q. Wang, R. Ke, T. Zhang, X. Ao, G. Zhang, Z. Liu, Y. Qian, F. Pan, I. Lynch, J. Wang and Y. Deng, *J. Energy Chem.*, 2024, **88**, 532–542.

181 J. Qian, W. A. Henderson, W. Xu, P. Bhattacharya, M. Engelhard, O. Borodin and J.-G. Zhang, *Nat. Commun.*, 2015, **6**, 6362.

182 Y.-X. Yao, X. Chen, C. Yan, X.-Q. Zhang, W.-L. Cai, J.-Q. Huang and Q. Zhang, *Angew. Chem., Int. Ed.*, 2021, **60**, 4090–4097.

183 Y. Jie, S. Wang, S. Weng, Y. Liu, M. Yang, C. Tang, X. Li, Z. Zhang, Y. Zhang, Y. Chen, F. Huang, Y. Xu, W. Li, Y. Guo, Z. He, X. Ren, Y. Lu, K. Yang, S. Cao, H. Lin, R. Cao, P. Yan, T. Cheng, X. Wang, S. Jiao and D. Xu, *Nat. Energy*, 2024, **9**, 987–998.

184 S. Li, Z. Luo, L. Li, J. Hu, G. Zou, H. Hou and X. Ji, *Energy Storage Mater.*, 2020, **32**, 306–319.

185 X.-Q. Zhang, X.-B. Cheng, X. Chen, C. Yan and Q. Zhang, *Adv. Funct. Mater.*, 2017, **27**, 1605989.

186 Y. Liu, D. Lin, Y. Li, G. Chen, A. Pei, O. Nix, Y. Li and Y. Cui, *Nat. Commun.*, 2018, **9**, 3656.

187 Z. Wang, L.-P. Hou, Z. Li, J.-L. Liang, M.-Y. Zhou, C.-Z. Zhao, X. Zeng, B.-Q. Li, A. Chen, X.-Q. Zhang, P. Dong, Y. Zhang, J.-Q. Huang and Q. Zhang, *Carbon Energy*, 2023, **5**, e283.

188 Q.-K. Zhang, S.-Y. Sun, M.-Y. Zhou, L.-P. Hou, J.-L. Liang, S.-J. Yang, B.-Q. Li, X.-Q. Zhang and J.-Q. Huang, *Angew. Chem., Int. Ed.*, 2023, **62**, e202306889.

189 M. S. Kim, Z. Zhang, P. E. Rudnicki, Z. Yu, J. Wang, H. Wang, S. T. Oyakhire, Y. Chen, S. C. Kim, W. Zhang, D. T. Boyle, X. Kong, R. Xu, Z. Huang, W. Huang, S. F. Bent, L.-W. Wang, J. Qin, Z. Bao and Y. Cui, *Nat. Mater.*, 2022, **21**, 445–454.

190 Y. Gao, X. Du, Z. Hou, X. Shen, Y.-W. Mai, J.-M. Tarascon and B. Zhang, *Joule*, 2021, **5**, 1860–1872.

191 P. Liu, L. Miao, Z. Sun, X. Chen, Y. Si, Q. Wang and L. Jiao, *Angew. Chem., Int. Ed.*, 2023, **62**, e202312413.

192 G. Li, Y. Gao, X. He, Q. Huang, S. Chen, S. H. Kim and D. Wang, *Nat. Commun.*, 2017, **8**, 850.

193 Y. Gao and B. Zhang, *Adv. Mater.*, 2023, **35**, 2205421.

194 Y. Li, W. Huang, Y. Li, A. Pei, D. T. Boyle and Y. Cui, *Joule*, 2018, **2**, 2167–2177.

195 A. Kolesnikov, M. Kolek, J. F. Dohmann, F. Horsthemke, M. Börner, P. Bieker, M. Winter and M. C. Stan, *Adv. Energy Mater.*, 2020, **10**, 2000017.

196 H. Kwon, H. Kim, J. Hwang, W. Oh, Y. Roh, D. Shin and H.-T. Kim, *Nat. Energy*, 2024, **9**, 57–69.

197 D. Lin, Y. Liu, Y. Li, Y. Li, A. Pei, J. Xie, W. Huang and Y. Cui, *Nat. Chem.*, 2019, **11**, 382–389.

198 A. Kolesnikov, D. Zhou, M. Kolek, J. P. B. Jimenez, P. Bieker, M. Winter and M. C. Stan, *J. Electrochem. Soc.*, 2019, **166**, A1400–A1407.

199 A. C. Kozen, C.-F. Lin, A. J. Pearse, M. A. Schroeder, X. Han, L. Hu, S.-B. Lee, G. W. Rubloff and M. Noked, *ACS Nano*, 2015, **9**, 5884–5892.

200 F. Ding, W. Xu, G. L. Graff, J. Zhang, M. L. Sushko, X. Chen, Y. Shao, M. H. Engelhard, Z. Nie, J. Xiao, X. Liu, P. V. Sushko, J. Liu and J.-G. Zhang, *J. Am. Chem. Soc.*, 2013, **135**, 4450–4456.

201 C. Jin, T. Liu, O. Sheng, M. Li, T. Liu, Y. Yuan, J. Nai, Z. Ju, W. Zhang, Y. Liu, Y. Wang, Z. Lin, J. Lu and X. Tao, *Nat. Energy*, 2021, **6**, 378–387.

202 M. Genovese, A. J. Louli, R. Weber, S. Hames and J. R. Dahn, *J. Electrochem. Soc.*, 2018, **165**, A3321–A3325.

203 T. M. Bond, J. C. Burns, D. A. Stevens, H. M. Dahn and J. R. Dahn, *J. Electrochem. Soc.*, 2013, **160**, A521–A527.

204 A. J. Smith, J. C. Burns, S. Trussler and J. R. Dahn, *J. Electrochem. Soc.*, 2010, **157**, A196–A202.

205 W. Yu, K.-Y. Lin, D. T. Boyle, M. T. Tang, Y. Cui, Y. Chen, Z. Yu, R. Xu, Y. Lin, G. Feng, Z. Huang, L. Michalek, W. Li, S. J. Harris, J.-C. Jiang, F. Abild-Pedersen, J. Qin, Y. Cui and Z. Bao, *Nat. Chem.*, 2025, **17**, 246–255.

206 A. S. Keefe, S. Buteau, I. G. Hill and J. R. Dahn, *J. Electrochem. Soc.*, 2019, **166**, A3272–A3279.

207 X. Lv, J. Liu, C. Li, F. Yu, D. Xiao, S. Zhao, Y. Wu and Y. Chen, *eScience*, 2024, DOI: **10.1016/j.esci.2024.100351**.

208 N. Yao, X. Chen, S.-Y. Sun, Y.-C. Gao, L. Yu, Y.-B. Gao, W.-L. Li and Q. Zhang, *Chem*, 2025, **11**, 1–7.

209 X. Chen, Y.-K. Bai, C.-Z. Zhao, X. Shen and Q. Zhang, *Angew. Chem., Int. Ed.*, 2020, **59**, 11192–11195.

210 T.-Z. Hou, W.-T. Xu, X. Chen, H.-J. Peng, J.-Q. Huang and Q. Zhang, *Angew. Chem., Int. Ed.*, 2017, **56**, 8178–8182.

211 M. Leskes, G. Kim, T. Liu, A. L. Michan, F. Aussenac, P. Dorffer, S. Paul and C. P. Grey, *J. Phys. Chem. Lett.*, 2017, **8**, 1078–1085.

212 B. Reif, S. E. Ashbrook, L. Emsley and M. Hong, *Nat. Rev. Methods Primers*, 2021, **1**, 2.

213 X. Zhang and H. Huo, *Magn. Reson. Lett.*, 2021, **1**, 142–152.

214 W. Zhang, P. Sayavong, X. Xiao, S. T. Oyakhire, S. B. Shuchi, R. A. Vilá, D. T. Boyle, S. C. Kim, M. S. Kim, S. E. Holmes, Y. Ye, D. Li, S. F. Bent and Y. Cui, *Nature*, 2024, **626**, 306–312.

215 F. Liu, R. Xu, Y. Wu, D. T. Boyle, A. Yang, J. Xu, Y. Zhu, Y. Ye, Z. Yu, Z. Zhang, X. Xiao, W. Huang, H. Wang, H. Chen and Y. Cui, *Nature*, 2021, **600**, 659–663.

216 C. Ma, S. Weng, Y. Zhang, X. Zhang, T. Liu, L. Liu, Z. Zhao, C. Liu, Z. Zhao, X. Wang, B. Wu, D. Mu and F. Wu, *Nano Lett.*, 2022, **22**, 9268–9274.

217 Y.-C. Gao, N. Yao, X. Chen, L. Yu, R. Zhang and Q. Zhang, *J. Am. Chem. Soc.*, 2023, **145**, 23764–23770.

218 X. Chen, X. Liu, X. Shen and Q. Zhang, *Angew. Chem., Int. Ed.*, 2021, **60**, 24354–24366.

219 Y.-C. Gao, Y.-H. Yuan, S. Huang, N. Yao, L. Yu, Y.-P. Chen, Q. Zhang and X. Chen, *Angew. Chem., Int. Ed.*, 2025, **64**, e202416506.

220 X. Liu, B.-B. Zou, Y.-N. Wang, X. Chen, J.-Q. Huang, X.-Q. Zhang, Q. Zhang and H.-J. Peng, *J. Am. Chem. Soc.*, 2024, **146**(48), 33012–33021.

221 C. Han, Y.-C. Gao, X. Chen, X. Liu, N. Yao, L. Yu, L. Kong and Q. Zhang, *InfoMat*, 2024, **6**, e12521.

222 J.-N. Liu, C.-X. Zhao, J. Wang, X.-Q. Fang, C.-X. Bi, B.-Q. Li and Q. Zhang, *Joule*, 2024, **8**, 1804–1819.

223 X. Li, D. Yu, V. S. Byg and S. D. Ioan, *J. Energy Chem.*, 2023, **82**, 103–121.